https://doi.org/10.5194/egusphere-2025-1370
Preprint. Discussion started: 3 April 2025

Deglaciation of the Sierra Nevada (USA) during Heinrich Event 1

Richard A. Becker[1], Aaron M. Barth[2], Shaun A. Marcott[3], Basil Tikoff[3], and Marc W. Caffee[4,5]

[1]Department of Earth and Environment, Boston University, 685 Commonwealth Ave, Boston, MA 02215, USA

[2]Department of Geology, Rowan University, 201 Mullica Hill Rd, Glassboro, NJ 08028, USA

[3]Department of Geoscience, University of Wisconsin-Madison, 1215 W Dayton St, Madison, WI 53706 USA

[4]Department of Physics and Astronomy, Purdue University, 525 Northwestern Ave, West Lafayette, IN 47907, USA

[5]Department of Earth, Atmospheric, and Planetary Sciences, Purdue University, 550 Stadium Mall Dr, West Lafayette, IN 47907, USA

Correspondence to: Richard A. Becker (rabecker@bu.edu)

https://doi.org/10.5194/egusphere-2025-1370
Preprint. Discussion started: 3 April 2025

Abstract (≤250 words)

A polar jet stream (PJS) split by the Laurentide Ice Sheet (LIS) is a well-established feature of Ice-Age atmospheric circulation. California's central Sierra Nevada Mountains (37–38° N) lie near the reconstructed position of the PJS's southern branch. Previous studies concluded that rapid deglaciation began here at ca. 16–15 ka after millennia of relatively stability at ~60% LGM length. However, this conclusion is largely based on the behavior of glaciers in a single valley, Bishop Creek Canyon. We report 31 new ^{10}Be samples from two new locations – Lyell Canyon and Mono Creek Canyon – and 26 recalculated ^{36}Cl dates from Bishop Creek Canyon (n = 57). These dates indicate rapid deglaciation began at 16.4 ± 0.8 ka and lasted for ca. 1.0 kyr. Placing two previously published paleoenvironmental reconstructions (Swamp Lake and McLean's Cave) with centennial-or-better-scale resolution on new age-depth models that provide age-uncertainty estimates, we find evidence for warming in the central Sierra Nevada at 16.4 ± 0.4 ka and drying at 16.20 ± 0.13 ka. Collectively, we interpret that rapid deglaciation began at 16.20 ± 0.13 ka. This timing is indistinguishable from that of Heinrich Event 1 (HE1), which occurred between 16.22 ± 0.04 ka and 16.04 ± 0.04 ka. We hypothesize that the Sierra Nevada's deglaciation was driven by a northward repositioning and focusing of the winter-storm track over western North America in response to PJS reunification, bringing warmer and drier weather to the central Sierra Nevada, and that PJS reunification occurred in response HE1 thinning the LIS.

Keywords

Polar Jet Stream, Laurentide Ice Sheet, Sierra Nevada Mountains, Yosemite National Park, Heinrich Event 1, Be-10, Cl-36, Atmospheric Reorganization

https://doi.org/10.5194/egusphere-2025-1370
Preprint. Discussion started: 3 April 2025

Graphical Abstract

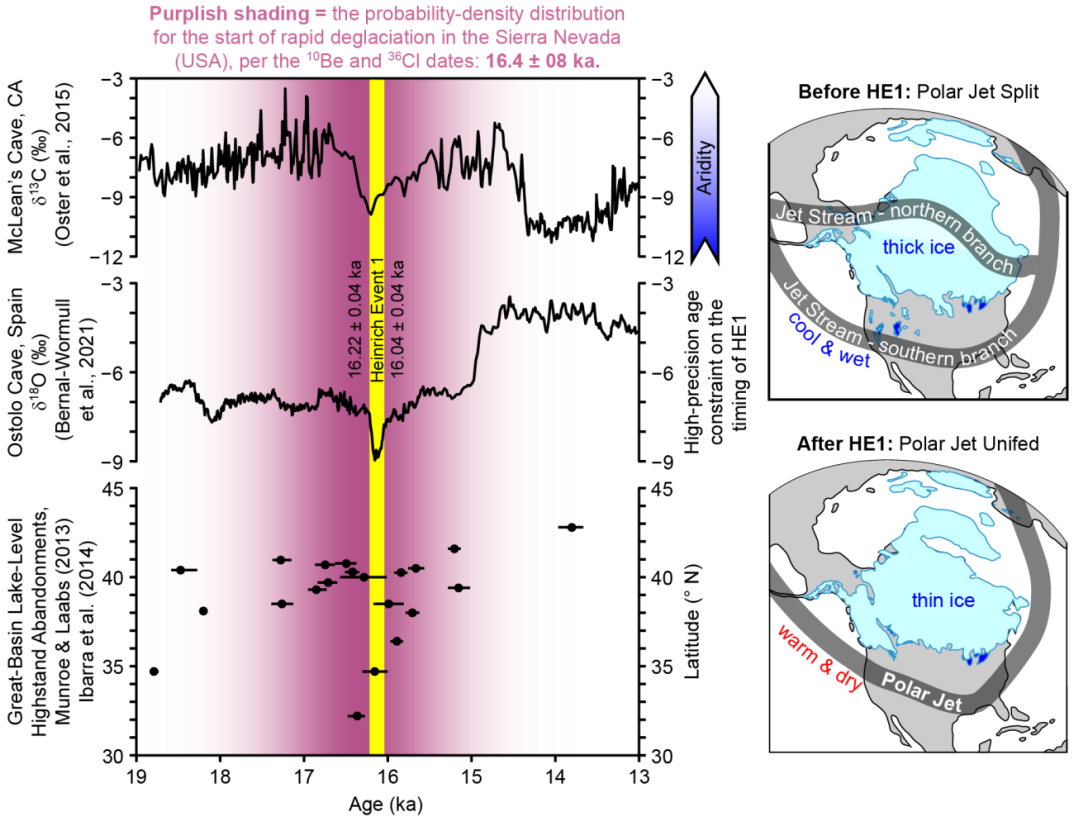

https://doi.org/10.5194/egusphere-2025-1370
Preprint. Discussion started: 3 April 2025

Short Summary (≤500 characters including spaces)

We report 31 new ^{10}Be and 26 recalculated ^{36}Cl dates from the Sierra Nevada Mountains (USA) and conclude that deglaciation's final and rapid phase began at 16.4 ± 0.8 ka. In comparing this timing with high-resolution regional paleoclimate proxies, we interpret that rapid deglaciation most likely began at 16.20 ± 0.13 ka, which is indistinguishable in timing from Heinrich Event 1. We interpret that the range's deglaciation was likely driven by a reunification of the polar jet stream at this time.

https://doi.org/10.5194/egusphere-2025-1370
Preprint. Discussion started: 3 April 2025

1. Introduction

Abrupt, millennial- and centennial-scale climate changes are a prominent characteristic of the last deglaciation in contrast to the relative stability of the Holocene (e.g., Mayewski et al., 2004; Denton et al., 2010; Clark et al., 2012; Shakun et al., 2012; Marcott et al., 2013). Numerous climate reversals of varying extents and magnitudes punctuated the latest Pleistocene, including the Younger Dryas (e.g., Mangerud et al., 1974; Mangerud, 2021), the Antarctic Cold Reversal (Jouzel et al., 1995), and the Heinrich and Dansgaard-Oeschger events (Heinrich, 1988; Dansgaard et al., 1993). Understanding these events – including their rate, timing, magnitude, geographical extent, duration, and ultimately their causes and consequences – has been a principal endeavor within Quaternary science (e.g., Alley, 2000; Ganopolski and Rahmstorf, 2001; Hemming, 2004; Douglass et al., 2006; Firestone et al., 2007; Ackert et al., 2008; Putnam et al., 2010a; Laabs et al., 2011; Rasmussen et al., 2014; Bahr et al., 2018; Barth et al., 2018; Pedro et al., 2018; Li and Born, 2019).

Field-based studies in the Sierra Nevada Mountains (USA) – such as geomorphic observations (Clark, 1976; Clark and Clark, 1995) and ^{10}Be, ^{26}Al, and ^{36}Cl surface-exposure dating (James et al., 2002; Phillips et al., 2009) – indicate that the range's glaciers responded strongly to a large and abrupt change in climate near the end of the last deglaciation. After Sierra Nevadan glaciers reached their greatest extents, broadly in-phase with the global Last Glacial Maximum (LGM; Phillips et al., 2009; Rood et al., 2011), they receded for several thousand years – with episodic advances superimposed on this general trend – before readvancing to ~60 % LGM-length. Glaciers in the Sierra Nevada rapidly melted following this readvance (Clark, 1976; Clark and Clark, 1995), receding from ~60 % LGM-length to <3 km length (0–23 % LGM-length) in "500 yr or less, and certainly less than 1000 yr" (Phillips et al., 2009, p. 1031).

https://doi.org/10.5194/egusphere-2025-1370
Preprint. Discussion started: 3 April 2025

This rapid ice recession may have been driven by a sharp reduction in precipitation either contemporaneously with or immediately following Heinrich Event 1 in the North Atlantic (Benson et al., 1996; Phillips et al., 1996).

This readvance and subsequent deglaciation suggest two reorganizations in atmospheric circulation over the northeastern Pacific Ocean. An earlier reorganization that brought cooler summers and/or wetter winters to the Sierra Nevada (driving the readvance) and a later, larger magnitude and more permanent reorganization that brought warmer summers and/or drier winters to the range (driving the deglaciation). This inference, derived from the Sierra Nevada's geomorphology, is supported by a regional reconstruction of sea-surface temperatures (SSTs) in the northeast Pacific that records cooling between ca. 18 ka and ca. 17 ka and warming after ca. 16.5 ka (Praetorius et al., 2020). Numerical modeling shows these cooler SSTs would have generated a deeper and longer lasting snowpack in the Sierra Nevada, with warmer SSTs having the opposite effect (Peteet et al., 1997).

The duration of the Tioga 4 deglaciation provides a maximum constraint on the duration of the second reorganization. However, the cosmogenic surface-exposure ages constraining the duration of this deglaciation to <500–1000 years (Phillips et al., 2009) are all associated with a single former glacier – the Bishop Creek Glacier – thus permitting the possibility that glacial recession was substantially slower (or more rapid) elsewhere in the range.

Here, we investigate the timing and duration of the final deglaciation in the Sierra Nevada with thirty-one new ^{10}Be-concentration measurements from two other drainage basins in the central portion of the range: (1) Tuolumne Meadows and Lyell Canyon in Yosemite National Park and (2) Lake Thomas A. Edison (which was Vermillion Valley prior to 1954 C.E.) and Mono Creek Canyon in the Sierra National Forest (Fig. 1). In converting these ^{10}Be

https://doi.org/10.5194/egusphere-2025-1370
Preprint. Discussion started: 3 April 2025

concentrations into surface-exposure ages, we consider multiple sources of uncertainty – especially with regards to the snow-shielding correction.

Additionally, we further constrain the timing and nature of the climate changes that drove the range's deglaciation – beyond the constraints imposed by the thirty-one new ^{10}Be dates – by reevaluating four legacy datasets. In particular, we (1) recalculate twenty-six ^{36}Cl dates on the timing and duration of the deglaciation within the vicinity of Bishop Creek Canyon (Phillips et al., 2009) using updated ^{36}Cl production rates and scaling schemes (e.g., Marrero, 2012; Lifton et al., 2014; Marrero et al., 2016), (2) recalibrate the age-depth model for the Swamp Lake paleoenvironmental reconstruction (Street et al., 2012) and (3) the radiocarbon dates reported by Munroe and Laabs (2013) and Ibarra et al. (2014) on the highstands of seventeen Great Basin Pleistocene lakes with IntCal 20 (Reimer et al., 2020) and Bchron 4.7.6 (Haslett and Parnell, 2008), and (4) recalculate the age-depth model for speleothem ML1 from McLean's Cave (Oster et al., 2015) using Bchron. We find evidence of warming and drying in the Sierra Nevada and adjacent regions ca. 16.2 ka and interpret these changes as resulting from a northward shift and focusing of the winter-storm track over North America in response to Heinrich Event 1, which is indistinguishable in timing from the start of the Tioga 4 deglaciation (Bernal-Wormull et al., 2021; Pérez-Mejías et al., 2021).

https://doi.org/10.5194/egusphere-2025-1370
Preprint. Discussion started: 3 April 2025

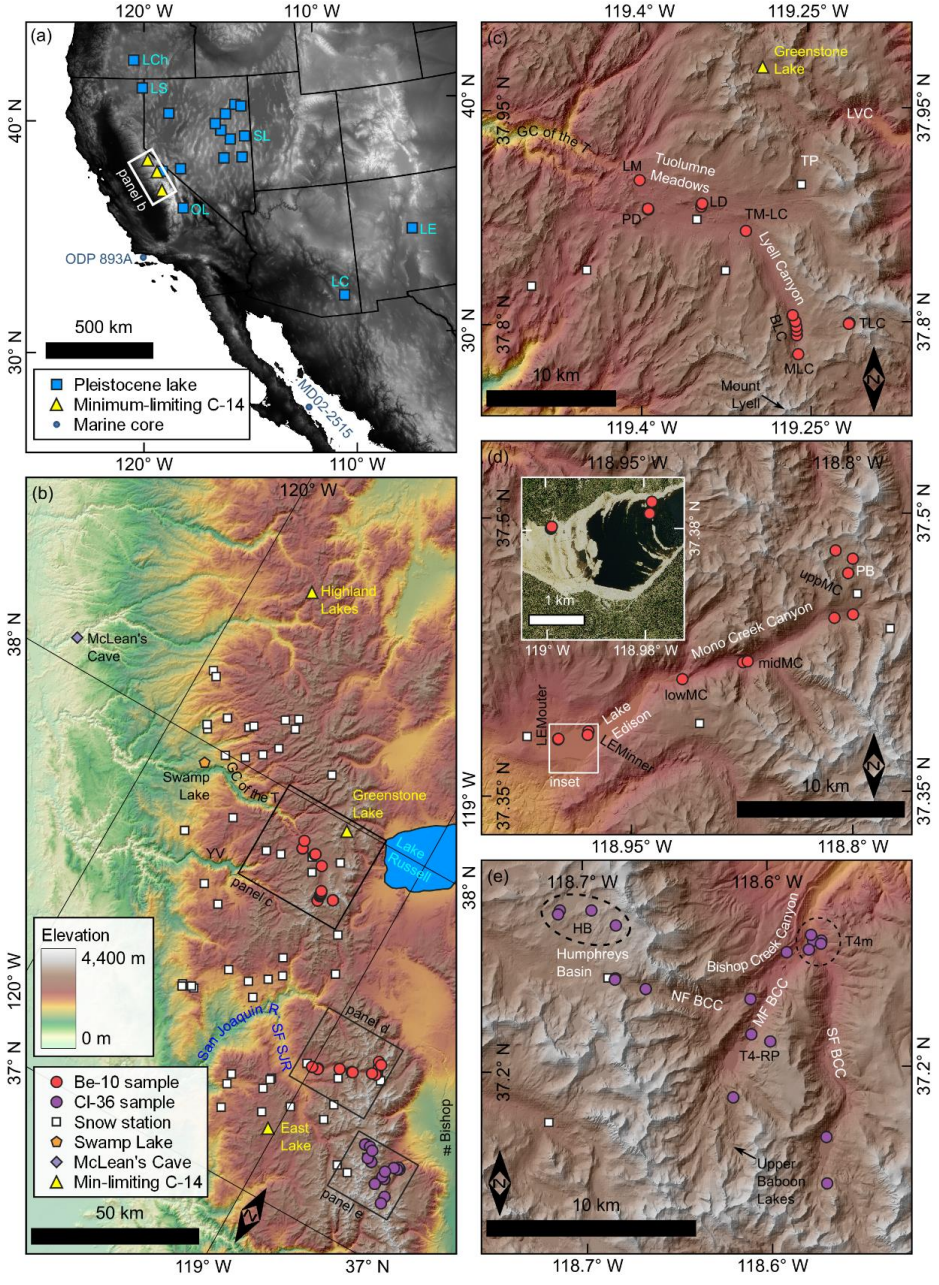

Figure 1. Maps showing the locations of the field areas and relevant data sets. **(a)** Location of the central Sierra Nevada Mountain range (panel b) in the western United States. Pleistocene lakes mentioned in the text are abbreviated as follows (north to south): LCh – Lake Chewaucan; LS – Lake Surprise; SL – Spring Lake; OL – Owens Lake; LE – Lake Estancia; and LC – Lake Cochise. For the names of the unlabeled lakes, please see Munroe and Laabs (2013). **(b)** Location of the field areas within the central Sierra Nevada. Abbreviations (north to south): GC

https://doi.org/10.5194/egusphere-2025-1370
Preprint. Discussion started: 3 April 2025

of the T – Grand Canyon of the Tuolumne River; YV – Yosemite Valley; and SF SJR – South Fork of the San Joaquin River. **(c)** Map of the Tuolumne Meadows and Lyell Canyon field area. Sampling-location abbreviations (from distal to proximal): LM – lower Tuolumne Meadows; PD – Pothole Dome; LD – Lembert Dome; TM-LC – unnamed roche moutonnée near the junction of Tuolumne Meadows with Lyell Canyon; BLC – bottom of Lyell Canyon; MLC – a mid-elevation within Lyell Canyon; and TLC – top of Lyell Canyon. Other abbreviations on panel c: LVC – Lee Vining Canyon; TP – Tioga Pass; and GC of the T – Grand Canyon of the Tuolumne River. **(d)** Map of the Lake Edison and Mono Creek Canyon field area. Sampling-location abbreviations (distal to proximal): LEMouter – the outermost moraine beneath Lake Edison (which was created in 1954 C.E. by the damming of Mono Creek and the flooding Vermillion Valley); LEMinner – the innermost moraine beneath Lake Edison; lowMC – lower Mono Creek; midMC – middle Mono Creek; and uppMC – upper Mono Creek. The other abbreviation on panel d: PB – Pioneer Basin. **(e)** 2014 aerial photo of the Lake Edison moraine complex, which was exposed by drought. **(f)** Map of Bishop Creek Canyon and vicinity. Sampling-location abbreviations: T4m – the Tioga 4 moraine; HB – Humphrey's Basin; and T4-RP – scattered sampling locations between the Tioga 4 moraine and the Recess Peak moraines. Other abbreviations on panel f: NF BCC – the North Fork of Bishop Creek Canyon; MF BCC – the Middle Fork of Bishop Creek Canyon; and SF BCC – the South Fork of Bishop Creek Canyon.

https://doi.org/10.5194/egusphere-2025-1370
Preprint. Discussion started: 3 April 2025

2. Regional setting

2.1. Physical geography of the Sierra Nevada

The Sierra Nevada is a ~600-km-long mountain range that parallels the western boundary of North America and hosts the highest elevation within the contiguous United States: Mt. Whitney at 4421 m (14,505 ft). The range formed during the Mesozoic as a result of subduction and arc magmatism (Gilluly, 1969; Hamilton, 1969; McPhillips and Brandon, 2010; Gabet, 2014). Quartz-bearing lithologies are abundant in the central and southern Sierra Nevada. That portion of the range is primarily granitic plutons with scattered metasedimentary and metavolcanic wall rocks (e.g., Bateman, 1992).

The range's length, orientation, and elevation make it an effective barrier to maritime air masses originating over the Pacific (e.g., Pandey et al., 1999). Furthermore, the range experiences a Mediterranean climate with dry summers and wet winters characterized by abundant snowfall. In Tuolumne Meadows for example (~2600 m elevation), 82% of its 1985–2017 precipitation arrived in the six months between November 1 and April 30 and 50% of that precipitation was snow (http://cdec.water.ca.gov). Average April snow depths at the elevation of Tuolumne Meadows were approximately 2 m between 1946 and 2008 (Fig. S1).

2.2. Glacial history of the Sierra Nevada

Within the Sierra Nevada, the last glaciation is termed the Tioga (Blackwelder, 1931) and is divided into five glacial advances: from oldest to youngest these are Tioga 1–4 (Phillips et al., 1996; Phillips et al., 2009) and then the comparatively minor Recess Peak (Birman, 1964; Clark and Gillespie, 1997). Tioga 1 predates both the local and global LGM (Phillips et al., 1996; Phillips et al., 2009); Tioga 2 marks the local LGM, which was ca. 24–21 ka (e.g., Clark et al., 2003; Phillips et al., 2009; Amos et al., 2010; Rood et al., 2011); Tioga 3 represents a readvance

https://doi.org/10.5194/egusphere-2025-1370
Preprint. Discussion started: 3 April 2025

to ~90 % the LGM ice extent ca. 23–20 ka (e.g., Schaefer et al., 2006; Phillips et al., 2009; Stock and Uhrhammer, 2010); and Tioga 4 marks a readvance to ~60 % LGM ice extent ca. 16 ka (Phillips et al., 2009; Phillips, 2016).

Rapid deglaciation of the Sierra Nevada began immediately after the Tioga 4 readvance (Clark and Gillespie, 1997). During the subsequent Recess Peak readvance, which culminated ca. 13.3 ka (Phillips, 2016; Marcott et al., 2019), northward-flowing glaciers deposited moraines ~0–3 km from their cirque headwalls (~1–23 % LGM length; Moore, 1981; Clark and Gillespie, 1997; Clark et al., 2003) while southward-facing cirques rarely contain Recess Peak moraines (Clark and Gillespie, 1997). This paper focuses the Tioga 4 readvance and the subsequent deglaciation.

2.2.1. Geomorphic constraints on the magnitude and duration of the Tioga 4 deglaciation

Multiple geomorphic observations suggest Sierra Nevadan glaciers rapidly melted following the Tioga 4 readvance (Birman, 1964; Clark, 1976; Clark and Clark, 1995). First, other than the relatively minor Recess Peak deposits (e.g., Birman, 1964; Clark and Gillespie, 1997; Phillips et al., 2009; Marcott et al., 2019), the innermost end moraines of the Sierra Nevada – the Tioga 4 moraines – are ~60 % the distance (15 and 22 km in Bishop Creek and Mono Creek Canyons, respectively) from the cirques to the Tioga 2 moraines (Clark, 1976; Clark and Clark, 1995; Phillips et al., 2009). Distal of ~60 %, end moraines are common and bedrock basins are typically sediment-filled; proximal of ~60 %, bedrock basins are water-filled, bedrock-outcrop exposure is excellent, and glacial sediments are primarily isolated boulders and till patches (Clark, 1976; Clark and Clark, 1995).

Second, within the Lake Edison moraine complex – which is an assemblage of approximately eleven end moraines in the Mono Creek drainage at 63–58 % LGM-glacier length

https://doi.org/10.5194/egusphere-2025-1370
Preprint. Discussion started: 3 April 2025

(24–22 km; Figs. 1d–e and 2) – till thickness systematically decreases from the outermost to innermost moraine; immediately behind the innermost moraine, till is absent for 4 km (Birman, 1964). Although Birman (1964) interpreted the decreased till thickness as a temporal evolution toward lower debris concentrations in the Late Pleistocene glaciers of the Sierra Nevada, it is also consistent with rapid deglaciation. Phillips (2016) correlated the entire Lake Edison moraine complex with the Tioga 4 glacial advance and used the elevation difference between the moraines and various unspecified cirque headwalls in the Mono Creek drainage to reconstruct an equilibrium-line altitude (ELA) of 2800 m for the Tioga 4 advance. Based on Pioneer Basin's cirque-floor elevation (~3400 m), this reconstruction implies the Tioga 4 deglaciation was driven by a ≥600 m ELA rise. This ELA rise is a minimum estimate because the climatological snowline may have risen above the elevation of the cirque floors.

https://doi.org/10.5194/egusphere-2025-1370
Preprint. Discussion started: 3 April 2025

Figure 2. A 1908 photograph by G. K. Gilbert of one of the moraines within what is now the Lake Edison moraine complex. Photo courtesy of the United States Geological Survey's (USGS's) Denver Library Photographic Collection; item identifier ggk03340.

https://doi.org/10.5194/egusphere-2025-1370
Preprint. Discussion started: 3 April 2025

Finally, upvalley from the Tioga 4 end moraines – and presumably within the footprint of the former Tioga 4 accumulation zone – low-relief ridges emanate from tributary-valley junctions and parallel the inferred direction of former ice flow (e.g., Birman, 1964, Plate 1). Clark (1976) observed numerous such ridges in the vicinity of Tuolumne Meadows (at ~30 % LGM-glacier length) and Clark and Clark (1995) observed similar ridges in the upper reaches of Mono Creek Canyon (at ~10 % LGM-glacier length). These low-relief, ice-flow parallel ridges are inferred to be medial moraines (Clark, 1976; Clark and Clark, 1995). Based on the presence of these medial moraines – and the absence of crosscutting end moraines and other ice-marginal landforms – Clark (1976) and Clark and Clark (1995) interpreted that Sierra Nevadan glaciers stagnated and rapidly melted at the end of the last glaciation.

2.2.2. Radiocarbon constraints on the timing of the Tioga 4 deglaciation

Phillips (2016) reviewed radiocarbon constraints on the timing of the Tioga 4 deglaciation and placed this event at 15.75 ± 0.5 ka (1 σ). This determination was based on three bulk-sediment radiocarbon dates from high-altitude ponds within the Tioga 4 glacial footprint (Fig. 1b). From north to south, and when calibrated with Calib 8.2 (Stuiver and Reimer, 1993) and IntCal20 (Reimer et al., 2020), these dates are 15.95 ± 0.29 ka from the Highland Lakes in the North Fork of the Stanislaus River drainage (13,270 ± 200 ^{14}C-yrs; Clark et al., 1995), 15.69 ± 0.09 ka from Greenstone Lake in the Lee Vining Creek drainage (13,090 ± 60 ^{14}C-yrs; Clark et al., 2003), and 16.13 ± 0.10 ka from East Lake in the North Fork of the Kings River drainage (13,400 ± 60 ^{14}C-yrs; Power, 1998; Fig. S2). Although a small dataset, these three dates span ~160 km of the Sierra Nevada and include locations north of, nearly adjacent to, and just south of the new ^{10}Be dates we report. As these radiocarbon dates are from the basal layers of high-elevation ponds – and there is no compelling evidence for the contaminating presence of "dead

https://doi.org/10.5194/egusphere-2025-1370
Preprint. Discussion started: 3 April 2025

carbon" (carbon without radiocarbon activity; a topic we discuss further in Sect. 5.2.1.) – these dates suggest widespread deglaciation of the Sierra Nevada by ca. 16 ka, or in Phillips's (2016) interpretation, at 15.75 ± 0.5 ka.

The youngest of these three minimum-limiting radiocarbon ages – the 15.69 ± 0.09 ka date from Greenstone Lake (Clark et al., 2003) – is especially relevant to this manuscript. Greenstone Lake is only 15–25 km north of Tuolumne Meadows and Lyell Canyon (Fig. 1c) and erratic boulders deposited during the Tioga 4 deglaciation indicate that the Tioga 4 ice divide was northeast of the modern hydrologic divide: ice flowed across Tioga Pass (TP on Fig. 1c) from what is now the Lee Vining Creek watershed and contributed to the former Tuolumne Glacier (Huber, 2007; Wahrhaftig et al., 2019). The bedrock geology requires these erratics to have come from ≤4 km of Greenstone Lake (Bateman et al., 1983). After crossing Tioga Pass, erratic boulder trains and streamlined landforms demonstrate (Wahrhaftig et al., 2019) these originally-near-Greenstone-Lake parcels of ice passed through Tuolumne Meadows ~1–2 km north of our sampling sites on Lembert Dome (LD on Fig. 1c) and in lower Tuolumne Meadows (LM on Fig. 1c).

As a result of the Greenstone Lake radiocarbon date's calibrated-age-uncertainty envelope, Greenstone Lake was both deglaciated and accumulating organic carbon by 15.42 ka (Fig. S2; Haslett and Parnell, 2008; R Core Team, 2024). Thus, the Greenstone Lake radiocarbon date (1) constrains the timing of deglaciation in a directly adjacent glacial system (that of Lee Vining Canyon; LVC on Fig. 1c) and (2) suggests that Tuolumne Meadows was almost certainly deglaciated (if not also revegetating) by 15.4 ka. We therefore adopt 15.4 ka as a minimum-limiting constraint on the timing of deglaciation in Tuolumne Meadows and 15.75 ± 0.5 ka

https://doi.org/10.5194/egusphere-2025-1370
Preprint. Discussion started: 3 April 2025

(Phillips, 2016) as the best estimate for the timing of deglaciation in the high-elevation lake basins elsewhere in the Sierra Nevada.

2.2.3 Chlorine-36 constraints on the timing and duration of the Tioga 4 deglaciation

Phillips et al. (2009) tested the geomorphic interpretation of an abrupt end to the last glaciation in the Sierra Nevada by ^{36}Cl-dating boulders and bedrock outcrops in the vicinity of Bishop Creek (Fig. 1f). Applying then-current exposure-age calculation methods (i.e., Phillips et al., 2001), five dates from the Tioga 4 moraine in the Middle Fork of Bishop Creek Canyon ("T4m" on Fig. 1e) yielded a mean age and standard deviation of 15.2 ± 1.0 ka, fifteen samples scattered between the Tioga 4 moraine and the Recess Peak moraines yielded a mean age and standard deviation of 14.7 ± 1.0 ka, and five samples from Humphreys Basin ("HB" on Fig. 1e), a broad collection of cirques west of the modern drainage divide, yielded a mean age and standard deviation of 15.2 ± 0.6 ka. Note that – although Humphreys Basin is west of the Sierra Crest – striations indicate the Tioga ice divide was 0.5–1.0 km west of the modern hydrologic divide in this location (Matthes, 1960; Phillips et al., 2009): Humphreys Basin contributed ice to both the San Joaquin and Bishop Creek Glaciers. Based on these dates, Phillips et al. (2009) concluded that the Tioga 4 deglaciation lasted <500–1000 years.

https://doi.org/10.5194/egusphere-2025-1370
Preprint. Discussion started: 3 April 2025

3. Materials and methods

3.1. Field areas and sample collection

We sampled thirty-one boulders in two drainages on the western slope of the Sierra Nevada (Figs. 1 and S3–S8; Tables S1–S3): (1) Tuolumne Meadows and Lyell Canyon in Yosemite National Park and (2) Lake Thomas A. Edison and Mono Creek Canyon in the Sierra National Forest.

3.1.1. *Tuolumne Meadows and Lyell Canyon*

We collected eighteen samples from seven locations along the flowline of the former Tuolumne Glacier in Yosemite National Park (Fig. 1c). From distal to proximal these are: (1) a single sample from a boulder on a bedrock slope above lower Tuolumne Meadows (LM; 24 km from the cirque headwall on Mount Lyell; Fig. S7), (2) three samples from Pothole Dome (PD; 22 km; Fig. S7), (3) three samples from Lembert Dome (LD; 18 km; Figs. S7 and S8), (4) a single sample from an unnamed roche moutonnée near the junction of Tuolumne Meadows with Lyell Canyon (TM-LC; 15 km; Fig. S6), (5) six samples from the bottom of Lyell Canyon (BLC; 6 km; ~2740 meters above sea level; Figs. S5 and S6), (6) a single sample from a mid-elevation within Lyell Canyon (MLC; 4 km; ~220 m above the bottom of Lyell Canyon; Fig. S5), and (7) three samples from the top of Lyell Canyon (TLC; 2 km; ~670 m above the bottom of Lyell Canyon; Fig. S5). Collectively, these eighteen boulders range from 46 cm to 2.5 m tall and half of the sampled surfaces (9 / 18) had glacial striations or similar evidence for no appreciable post-glacial weathering (Table S1).

These samples provide minimum constraints on the timing and duration of the Tioga 4 deglaciation in the Tuolumne drainage because the location of the Tuolumne Glacier's Tioga 4 terminus is unknown and thus undated. Based on the Tuolumne Glacier's LGM length (94 km;

https://doi.org/10.5194/egusphere-2025-1370
Preprint. Discussion started: 3 April 2025

Dühnforth et al., 2010) and other Tioga 4 moraines within the Sierra Nevada being located at ~60 % LGM length (Clark, 1976; Clark and Clark, 1995; Phillips et al., 2009), the Tuolumne Glacier's Tioga 4 terminus was likely in the lower reaches of the Grand Canyon of the Tuolumne (Fig. 1b). If so, ice-marginal landforms recording the position of the Tuolumne Glacier's Tioga 4 terminus may not have been preserved, given the Canyon's steep slopes. We note that an analogous situation was documented in Utah's steep-walled Big Cottonwood Canyon (Quirk et al., 2018).

3.1.2. *Lake Thomas A. Edison and Mono Creek Canyon*

We collected thirteen samples from five locations along the flowline of the former Mono Creek Glacier in the Sierra National Forest (Figs. 1d). From distal to proximal these are: (1) three samples from the outermost end moraine beneath Lake Thomas A. Edison (LEMouter; 24 km from the cirque headwall in Pioneer Basin; Figs. S4 and S5), (2) two samples from the innermost end moraine beneath Lake Edison (LEMinner; 22 km; Fig. S4), (3) a single sample from the lower portion of Mono Creek Canyon (lowMC; 15 km; Fig. S4), (4) two samples from the middle portion of Mono Creek Canyon (midMC; 11 km; Figs. S3 and S4), and (5) five samples from the upper portion of Mono Creek Canyon (uppMC; 1–5 km; Fig. S3). Note that Lake Edison was created in 1954 C.E. with the construction of the Vermillion Valley Dam and that approximately nine additional end moraines lie between the outermost and innermost Lake Edison moraines (Figs. 1d, 2, and S9). Collectively, these thirteen boulders range from 35 cm to 2.4 m and 25 % of the sampled surfaces had striations or glacial polish indicating little-to-no post-glacial erosion (Table S1).

https://doi.org/10.5194/egusphere-2025-1370
Preprint. Discussion started: 3 April 2025

3.2. *Laboratory preparation*

Samples were prepared at the University of Wisconsin-Madison. Collected rocks were crushed to 425–841 μm, processed through a Frantz LB-1 Magnetic Barrier Separator to remove magnetic grains, and etched in solutions of 2 % HF and 2 % HNO_3 while rotating on an APW Wyott HR-50. Quartz purity was measured by ICP-AES analysis prior to ion exchange chromatography. Samples with ≤200 ppm Al were dissolved in concentrated HF and HNO_3, spiked with a ^{9}Be carrier solution (OSU-White; Table S3), and dried. Beryllium fluoride was converted into $BeCl_2$ by repeatedly dissolving and drying the samples in $HClO_4$ (≥4x) before redissolving them in 8 M HCl. Iron, Ti, and Ca were removed with anion column chromatography (Bio-Rad AG1-X8 100–200 mesh chloride-form resin) and NH_4OH precipitations. The Be fraction was separated using cation chromatography (Bio-Rad AG50W-X8 100–200 mesh hydrogen-form resin) and precipitated in centrifuge tubes at a pH of ~8.5 by adding NH_4OH. Finally, the samples were dried in quartz crucibles on a hotplate at incremental heating steps of ~55 °C, ~70 °C, and ~180 °C before being incinerated at ~900 °C to produce BeO, which was mixed with Nb and packed into AMS targets. Isotopic ratios were measured at PRIME Lab, Purdue University, in relation to the 07KNSTD standard (Table S3).

3.3. *Selection of legacy data*

To complement the new ^{10}Be samples from Yosemite National Park and the Sierra National Forest, we include in our analysis twenty-six ^{36}Cl samples (Tioga 4) reported by Phillips et al. (2009) from the vicinity of Bishop Creek (Fig. 1e): the five boulder samples from the crest of the Tioga 4 moraine, sixteen boulder and bedrock measurements from locations between the Tioga 4 and Recess Peak moraines, and the five boulder samples from Humphreys Basin. Phillips et al. (2009) reported two additional ^{36}Cl measurements on a single sample

https://doi.org/10.5194/egusphere-2025-1370
Preprint. Discussion started: 3 April 2025

(BPCR91-11) from a roche moutonnée 1.2 km behind the Tioga 4 moraine – but both ages were anomalously old (ca. 22 ka) and we preemptively excluded this sample from our reanalysis. We also exclude the twenty-three bedrock ^{10}Be samples reported by Dühnforth et al. (2010) from Tuolumne Meadows and Lyell Canyon because uncertainties regarding the degree of inheritance and snow shielding. These samples were collected from small bedrock protrusions (e.g., roche moutonnées) and the heights of these protrusions were not reported. Additionally, we exclude the one ^{10}Be date and nine ^{26}Al dates reported by James et al. (2002) on the final deglaciation of the northwestern Sierra Nevada because of imprecision in these early cosmogenic dates.

3.4. Snow-shielding correction

Snow-shielding corrections for the thirty-one new ^{10}Be samples from Yosemite National Park and the Sierra National Forest were calculated using the historical relationship (ca. 1946–2008 C.E.) between monthly average snow water equivalent (SWE) and elevation (Fig. S21), the modern relationship between average snowpack density and SWE (Fig. S22c), and equation 3.76 from Gosse and Phillips (2001):

$$S_{snow} = \frac{1}{12}\sum_{i}^{12} e^{-\left(\frac{\left(z_{snow,i} - z_{sample}\right)\rho_{snow,i}}{\Lambda_{f,e}}\right)}, \quad (1)$$

where $z_{snow,i}$ is monthly average snow depth, z_{sample} is boulder height, $\rho_{snow,i}$ is monthly average snow density, and $\Lambda_{f,e}$ is the effective attenuation length of the cosmogenic ray flux. The historical relationship between monthly average SWE and elevation (Fig. S21) was derived from all the active California Department of Water Resources (CA DWR) snow-monitoring stations in the drainage basins of the Tuolumne, Merced, and San Joaquin Rivers with at least ten years of observations for a particular month (Fig. 1b; Tables S4–S6). The median number of stations over the six snowiest months (December through May) is forty-five. The relationship between average snowpack density and SWE (Fig. S22c) was derived from 15,971 daily observations of

https://doi.org/10.5194/egusphere-2025-1370
Preprint. Discussion started: 3 April 2025

snow depth and SWE within these three drainage basins. We propagated uncertainties in boulder height, snow depth, and snow density into the shielding uncertainties (Table S1). We assume historical snow depths and densities are representative of the post-glacial interval and do not apply a time-evolving snow-shielding correction (e.g., Ye et al., 2023). Additional details about how we calculated the snow-shielding corrections are in the supplement (Sect. S.5.).

For the twenty-six legacy ^{36}Cl dates on the Tioga 4 ice advance and subsequent deglaciation from the vicinity of Bishop Creek, we used the snow-shielding correction factors reported by Phillips et al. (2009), which they calculated using Eq. 1 in conjunction with data from CA DWR snow-monitoring stations near Bishop Creek.

3.5. Exposure-age calculations

Surface-exposure ages were calculated using version 3.0.2 of the Balco et al. (2008) calculator with the underlying constants last updated on 3 March 2024 (the "Version 3" calculator), CRONUScalc 2.0 (Marrero et al., 2016), and CREp (Martin et al., 2017). CREp does not report a version number (Dr. Pierre-Henri Blard, personal communication, 16 July 2018); these ages were calculated on 3 March 2024. While employing additional calculators provides little-to-no leverage on the problem of systematic uncertainties within ^{10}Be dating – which are chiefly related to the spatial and temporal scaling of ^{10}Be production rates (e.g., Balco, 2011; Borchers et al., 2016) – we are unaware of any scientific rationale for preferring the results of one calculator over another. Our rational for providing multiple calculations is to assess the sensitivity of the various calculators on our primary conclusions.

Across all three calculators (Balco et al., 2008; Marrero et al., 2016; Martin et al., 2017) we used LSDn scaling (Lifton et al., 2014) and the ERA-40 atmospheric model (Uppala et al., 2005). We preferred the LSDn scaling model over the time independent (St) and dependent (Lm)

https://doi.org/10.5194/egusphere-2025-1370
Preprint. Discussion started: 3 April 2025

versions of Lal-Stone scaling (Nishiizumi et al., 1989; Lal, 1991; Stone, 2000; Balco et al., 2008) because of LSDn's grounding in first principles and its ability to explain ^{10}Be concentrations that appear supersaturated with St scaling (Balco, 2016). With regards to the atmospheric model, the Version 3 calculator and CRONUScalc 2.0 are both hardcoded to use ERA-40; for CREp, we elected to use ERA-40 over the U.S. standard atmosphere (NOAA et al., 1976) because of ERA-40's greater fidelity to observed atmospheric pressures (Balco, 2015). As for geomagnetic field reconstruction, the Version 3 calculator is hardcoded to use Lifton (2016) while CRONUScalc 2.0 is hardcoded to use Lifton et al. (2014); for CREp, we adopted Lifton (2016).

We used each calculator's default production-rate-calibration dataset. For the Version 3 calculator and for CRONUScalc 2.0 this is the CRONUS-Earth primary ^{10}Be calibration dataset (Putnam et al., 2010b; Marrero, 2012; Kelly et al., 2015; Lifton et al., 2015; Phillips et al., 2016). As such, the Version 3 calculator uses a non-dimensional LSDn fitting parameter of 0.838 ± 0.048; it does not report a sea-level high-latitude (SLHL) production rate in atoms g^{-1} quartz yr^{-1}. Balco (2018) discusses this reporting decision. CRONUScalc 2.0 uses a SLHL ^{10}Be production rate of 3.92 ± ~0.33 atoms g^{-1} quartz yr^{-1} (Borchers et al., 2016; Marrero et al., 2016); it does not report an LSDn fitting parameter. CREp's default ^{10}Be-production-rate dataset is every published production-rate-calibration study without a major demonstrated flaw (Martin et al., 2017); on 3 March 2024 CREp used a SLHL production rate of 4.06 ± 0.23 atoms g^{-1} quartz yr^{-1} based on the work of Gosse et al. (1995), Farber et al. (2005), Balco et al. (2009), Putnam et al. (2010a), Fenton et al. (2011), Kaplan et al. (2011), Goehring et al. (2012), Young et al. (2013), Claude et al. (2014), Kelly et al. (2015), Martin et al. (2015), Small and Fabel (2015), Stroeven et al. (2015), and Putnam et al. (2019). CREp also does not report an LSDn scaling factor. While we focus this manuscript's interpretations on the ages inferred from the globally distributed

https://doi.org/10.5194/egusphere-2025-1370
Preprint. Discussion started: 3 April 2025

production-rate datasets, we also consider the impact on our interpretations of calculating the exposure ages with ^{10}Be production rates derived from the Promontory Point calibration site (Sect. 5.2.2; Lifton et al., 2015).

For the Version 3 calculator and CREp (Martin et al., 2017), the reported internal age uncertainties solely reflect ^{10}Be concentration uncertainty while the external uncertainties reflect ^{10}Be concentration and production-rate uncertainties. For CRONUScalc 2.0 (Marrero et al., 2016), the internal age uncertainties reflect twelve sources of uncertainty (Tables S1–S3): sample latitude, longitude, elevation, thickness, density, topographic shielding, erosion rate, ^{10}Be concentration, attenuation length, boulder height, modern SWE by month as a function of elevation (Fig. S21), and average snowpack density as a function of SWE (Fig. S22c). The external age uncertainties we report for CRONUScalc include these same twelve sources of uncertainty plus the production rate and scaling uncertainties (Borchers et al., 2016).

We adjusted all reported surface-exposure ages such that they are relative to 1950 C.E. in order to facilitate comparison with the calibrated radiocarbon dates. (The Version 3 calculator and CREp report exposure durations prior to sampling; CRONUScalc 2.0 reports exposure ages relative to 2010 C.E.) We also rounded all cosmogenic age uncertainties mentioned in the text up to the next highest tenths position [when reported in units of kiloannum (ka)] in order to avoid rounding the uncertainties down to lower values than justifiable (e.g., the 0.434 ka uncertainty for sample TM14-15 in the CRONUScalc column of Table 1 becomes 0.5 ka in the text).

3.6. Outlier identification and group-age and uncertainty calculations

For the locations where we report or recalculate at least three samples, we identify outliers using an approach inspired by Tulenko et al. (2022): we first calculate the arithmetic mean and standard deviation of all the surface-exposure ages from a particular location and then

https://doi.org/10.5194/egusphere-2025-1370
Preprint. Discussion started: 3 April 2025

assess – within the CRONUScalc 2.0 ages – whether any samples deviate by more than twice their internal age uncertainty (>2 σ) from their group's arithmetic mean. If so, we label the most extreme deviator from the arithmetic mean an outlier across all three calculators, recalculate the mean, and assess whether any sample still deviates by more than two standard deviations from this new mean. If so, we iterate the outlier identification and rejection protocol described above until all remaining samples are within twice their internal age uncertainty of their group's mean age. For the dataset we report here, iterating this approach more than twice was not required and we only reject four samples out of the forty-nine samples (8 %) from locations where we report three or more samples.

For the locations where we report two or fewer samples, we identify outliers using geomorphic relative-age relationships with the larger sampling groups.

We use the CRONUScalc results to identify outliers for three reasons. First, applying this algorithm across all three calculators might result in some samples being rejected within one calculator's results and not those of another. Second, using the CRONUScalc results for outlier identification is the most conservative implementation of this outlier-identification protocol because the CRONUScalc results include more sources of uncertainty than the results of the other two calculators. Finally, as of this writing, CRONUScalc is the only calculator of the three that calculates ^{36}Cl surface-exposure ages (although we acknowledge that both the Version 3 calculator and CREp have ^{36}Cl-calculation methods in development). Thus, at the time of writing, using the CRONUScalc results to identify outliers provides analytic uniformity across the combined dataset of ^{10}Be and ^{36}Cl ages.

https://doi.org/10.5194/egusphere-2025-1370
Preprint. Discussion started: 3 April 2025

To calculate each sampling location's external age uncertainty, we multiplied each group's standard deviation by the average ratio of the external-to-internal age uncertainties in that group.

3.7. Deglaciation duration calculations

We calculated deglaciation's duration within Lyell, Mono Creek, and Bishop Creek Canyons using 1 x 10^5 trial Monte Carlo simulations. As input, these simulations used each sampling group's mean surface-exposure age and the standard deviation of the ages in that group. We then filtered the results of these Monte Carlo simulations and identified trials with simulated deglaciation ages consistent with the geomorphic relative-age requirements of the sampling sites (see Sect. S.6.).

3.8. Recalibration of previously published datasets

We used IntCal20 (Reimer et al., 2020) and the R package Bchron 4.7.6 (Haslett and Parnell, 2008; R Core Team, 2024) to recalibrate the radiocarbon ages in the ca. 18–10 ka portion of the Swamp Lake paleoenvironmental reconstruction (Street et al., 2012) and the radiocarbon ages that constrain the timing of Great Basin pluvial-lake highstands (Munroe and Laabs, 2013; Ibarra et al., 2014). We also used Bchron to construct a new age-depth model for speleothem ML1 from McLean's Cave (Oster et al., 2015). Our goal with the new age-depth models was to provide age uncertainties for the undated horizons in the Swamp Lake core and in speleothem ML1, as the original age-depth models do not provide age uncertainties at these depth increments.

https://doi.org/10.5194/egusphere-2025-1370
Preprint. Discussion started: 3 April 2025

4. Results

4.1. *New ^{10}Be dates from Tuolumne Meadows and Lyell Canyon*

We report eighteen new ^{10}Be samples from Tuolumne Meadows and Lyell Canyon in Yosemite National Park. After rejecting three outliers (Sect. S.7.), the fifteen remaining samples yield ages ranging 15.5–13.9 ka (Version 3 calculator), 16.4–14.7 ka (CRONUScalc 2.0), and 16.3–14.7 ka (CREp; Table 1). Across all three calculators, the location with the oldest surface-exposure age is lower Tuolumne Meadows (the most distal sampling site) and the youngest location is the bottom of Lyell Canyon (an intermediate location, but the site with the greatest ice thickness). In the Version 3 results, the sample (TM14-15) from lower Tuolumne Meadows has an age of 15.2 ± 0.3 ka (1 σ internal-age uncertainty) and the six samples from the bottom of Lyell Canyon have a mean and standard deviation of 14.4 ± 0.3 ka (Fig. 3b; Table 2). In contrast, CRONUScalc and CREp produce ages and internal uncertainties of 16.0 ± 0.5 ka and 16.0 ± 0.3 ka, respectively, for the sample from lower Tuolumne Meadows – and means and standard deviations of 15.1 ± 0.2 ka and 15.1 ± 0.3 ka, respectively, for the six samples from the bottom of Lyell Canyon (Fig. 3c–d; Table 2). Thus, CRONUScalc and CREp are producing surface-exposure ages for these samples that are ca. 0.8 kyr (5 %) older than the ages produced by the Version 3 calculator.

However, all three calculators produce nearly identical median estimates for the duration of the Tioga 4 deglaciation in Tuolumne Meadows and Lyell Canyon (i.e., the age difference between the lower Tuolumne Meadows sample and the mean age of the samples from the bottom of Lyell Canyon): 0.8 kyr with a 95 % confidence range of 0.2–1.5 kyr (Version 3 calculator), 0.9 kyr with a 95 % confidence range of 0.1–1.9 kyr (CRONUScalc 2.0; Fig. 3i), and 0.9 kyr with a 95 % confidence range of 0.3–1.5 kyr (CREp; Fig. 3j).

https://doi.org/10.5194/egusphere-2025-1370
Preprint. Discussion started: 3 April 2025

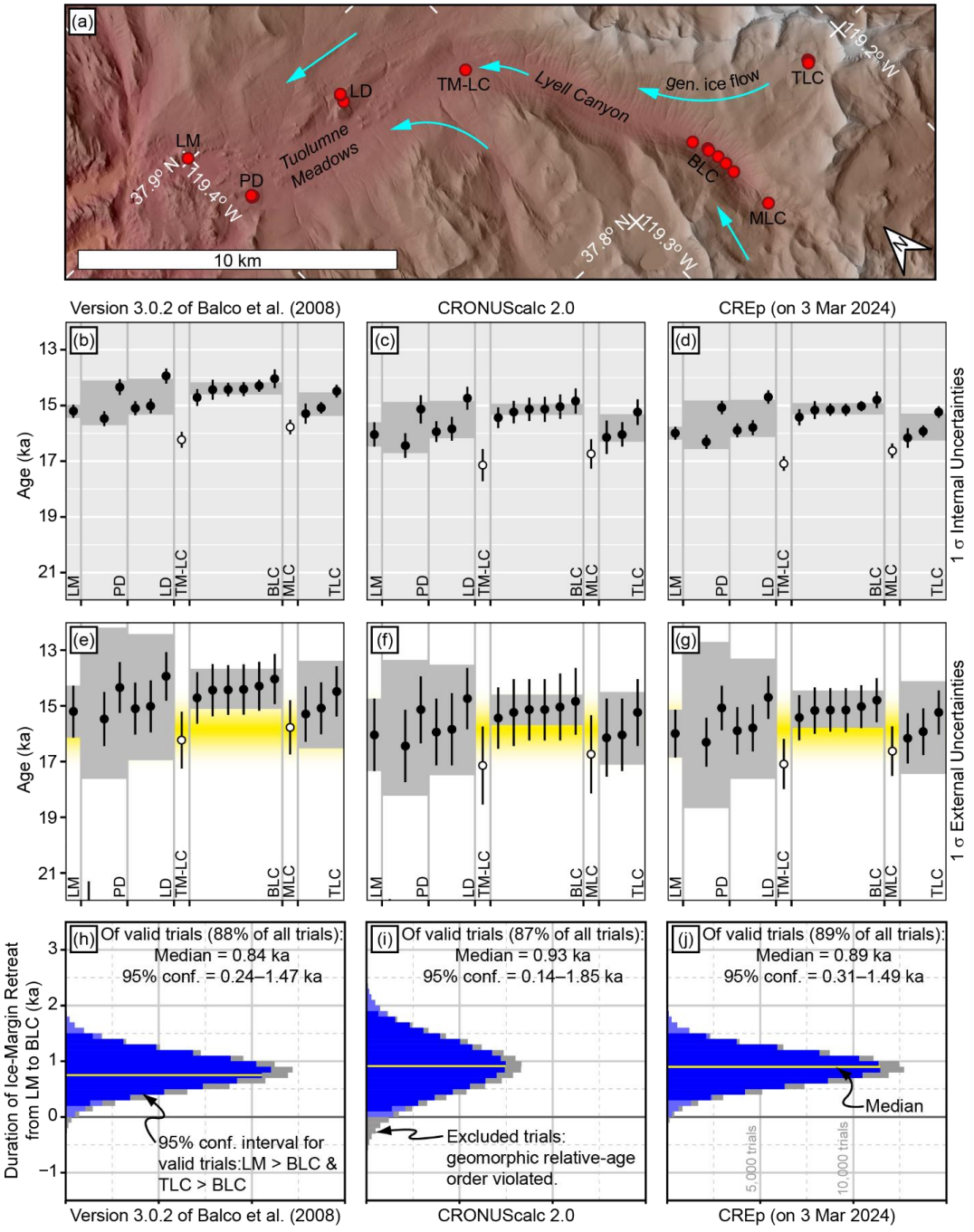

Figure 3. Sampling locations in the Tuolumne Meadows and Lyell Canyon field area, along with the surface-exposure ages and deglaciation durations inferred from those samples. **(a)** Sampling locations in Tuolumne Meadows and Lyell Canyon. Sampling-location abbreviations (from distal to proximal): LM – lower Tuolumne Meadows; PD – Pothole Dome; LM – Lembert

https://doi.org/10.5194/egusphere-2025-1370
Preprint. Discussion started: 3 April 2025

Dome; TM-LC – an unnamed roche moutonnée near the junction of Tuolumne Meadows with Lyell Canyon; BLC – the bottom of Lyell Canyon; MLC – a mid-elevation within Lyell Canyon; and TLC – the top of Lyell Canyon. **(b–d)** The ^{10}Be surface-exposure ages and 1 σ internal uncertainties. The gray boxes are the mean age of the retained ^{10}Be ages plus/minus one standard deviation. Rejected outliers are depicted with hollow symbols. Note that the extreme outlier (ca. 22–25 ka) from Pothole Dome (TM14-13) is outside the age range shown here. **(e–g)** The surface-exposure ages and 1 σ external uncertainties. The yellow shading's intensity represents the relative probability of deglaciation, according to Phillip's (2016) interpretation of the minimum-limiting radiocarbon dates. **(h–j)** Histograms for the duration of deglaciation. Each histogram is based on a 1 x 10^5 trial Monte Carlo simulation. We defined "valid" trials as those where the simulated deglaciation age of lower Tuolumne Meadows (LM) and the top of Lyell Canyon (TLC) were both older than the bottom of Lyell Canyon's (BLC's) simulated deglaciation age.

https://doi.org/10.5194/egusphere-2025-1370
Preprint. Discussion started: 3 April 2025

501 **Table 1.** Individual ^{10}Be and ^{36}Cl sample surface-exposure ages across the three calculators.

Calculator:	Balco et al. (2008) v. 3.0.2 (with 3 Mar 2024 constants)			Marrero et al. (2016) CRONUScalc 2.0			Martin et al. (2017) CREp (on 3 Mar 2024)		
Sample name	Age (ka)	Int. Err. (ka)	Ext. Err. (ka)	Age (ka)	Int. Err. (ka)	Ext. Err. (ka)	Age (ka)	Int. Err. (ka)	Ext. Err. (ka)
New Be-10 samples from Tuolumne Meadows and Lyell Canyon									
Top of Lyell Canyon (TLC)									
C2-Boulder1	15.085	0.206	0.932	16.040	0.436	1.300	15.928	0.210	0.840
C2-Boulder2	15.294	0.364	0.991	16.140	0.598	1.400	16.168	0.350	0.900
UpLy-12-10	14.484	0.228	0.902	15.240	0.460	1.200	15.238	0.210	0.790
Mid-elevation within Lyell Canyon (MLC)									
TM14-01	*15.773*	*0.265*	*0.975*	*16.740*	*0.525*	*1.400*	*16.626*	*0.260*	*0.890*
Bottom of Lyell Canyon (BLC)									
LoLy-11-08	14.436	0.357	0.940	15.240	0.402	1.200	15.169	0.320	0.830
TM14-02	14.432	0.244	0.892	15.140	0.418	1.100	15.146	0.220	0.780
TM14-03	14.715	0.301	0.925	15.440	0.367	1.100	15.426	0.290	0.810
TM14-04	14.296	0.215	0.877	15.040	0.438	1.200	15.026	0.180	0.770
TM14-05	14.040	0.335	0.900	14.840	0.454	1.200	14.796	0.300	0.790
TM14-06	14.414	0.252	0.904	15.140	0.449	1.100	15.156	0.220	0.790
An unnamed roche moutonnée between Tuolumne Meadows and Lyell Canyon (TM-LC)									
TM14-07	*16.233*	*0.284*	*1.019*	*17.140*	*0.575*	*1.400*	*17.086*	*0.260*	*0.900*
Pothole Dome in Tuolumne Meadows (PD)									
TM14-11	14.339	0.287	0.910	15.140	0.510	1.200	15.076	0.240	0.800
TM14-12	15.473	0.269	0.970	16.440	0.442	1.300	16.306	0.240	0.880
TM14-13	*22.761*	*0.474*	*1.460*	*23.940*	*0.997*	*2.000*	*23.866*	*0.430*	*1.250*
Lower Tuolumne Meadows (LM)									
TM14-15	15.207	0.239	0.936	16.040	0.434	1.300	15.996	0.230	0.860
Lembert Dome in Tuolumne Meadows (LD)									
TM14-16	*13.941*	*0.271*	*0.872*	*14.740*	*0.413*	*1.100*	*14.696*	*0.240*	*0.770*
TM14-17	15.019	0.264	0.931	15.840	0.430	1.300	15.796	0.270	0.840
TM14-18	15.098	0.249	0.932	15.940	0.370	1.200	15.896	0.250	0.850
New Be-10 samples from Lake Edison and Mono Creek Canyon									
Pioneer Basin and upper Mono Creek Canyon (uppMC)									
MR-14-03	14.963	0.208	0.925	15.840	0.343	1.200	15.796	0.210	0.820
MR-14-04	14.861	0.304	0.945	15.640	0.396	1.200	15.666	0.300	0.820
MR-14-05	14.657	0.226	0.901	15.440	0.385	1.200	15.416	0.210	0.780
MR-14-06	14.863	0.325	0.952	15.740	0.611	1.300	15.656	0.320	0.830
MR-14-07	14.699	0.292	0.932	15.440	0.420	1.200	15.456	0.280	0.810
Mid Mono Creek Canyon (midMC)									
MR-13-02	*20.077*	*0.312*	*1.234*	*21.040*	*0.505*	*1.400*	*21.027*	*0.270*	*1.000*
MR-14-08	*17.871*	*0.252*	*1.108*	*18.840*	*0.536*	*1.400*	*18.826*	*0.230*	*0.950*
Lower Mono Creek Canyon (lowMC)									
MR-13-01	15.136	0.433	1.009	16.040	0.594	1.400	15.997	0.420	0.920
Innermost moraine beneath Lake Edison (LEMinner)									
LEM-14-14	15.534	0.366	1.005	16.440	0.532	1.400	16.406	0.340	0.910
LEM-14-15	15.647	0.365	1.011	16.640	0.574	1.300	16.526	0.350	0.910
Outermost moraine beneath Lake Edison (LEMouter)									
LEM-16-28	18.579	0.377	1.184	19.540	0.552	1.400	19.524	0.340	1.010
LEM-16-29	*4.703*	*0.210*	*0.351*	*4.860*	*0.205*	*0.350*	*4.964*	*0.200*	*0.310*
LEM-16-30	19.421	0.336	1.221	20.340	0.520	1.400	20.374	0.290	1.010
Recalculated Cl-36 samples from Bishop Creek Canyon and vicinity (from Phillips et al., 2009)									
Tioga 4 moraine within the Middle Fork of Bishop Creek Canyon (T4m)									
BpCR97-8	N.A.	N.A.	N.A.	14.740	0.869	1.500	N.A.	N.A.	N.A.
BpCR97-9	N.A.	N.A.	N.A.	16.840	0.977	1.700	N.A.	N.A.	N.A.
BpCR97-13	N.A.	N.A.	N.A.	17.040	0.927	1.800	N.A.	N.A.	N.A.
BpCR97-14	N.A.	N.A.	N.A.	16.340	1.023	1.900	N.A.	N.A.	N.A.
BpCR97-15	N.A.	N.A.	N.A.	16.440	0.996	1.800	N.A.	N.A.	N.A.
Scattered boulders and bedrock outcrops between the Tioga 4 (T4m) and Recess Peak moraines in Bishop Creek Canyon (SB&O)									
BpCr95B-6(99)	N.A.	N.A.	N.A.	14.940	0.815	1.400	N.A.	N.A.	N.A.
BPCR96-1	N.A.	N.A.	N.A.	14.640	0.734	1.500	N.A.	N.A.	N.A.
BpCr96-16	N.A.	N.A.	N.A.	16.640	1.164	1.500	N.A.	N.A.	N.A.
BpCr96-17	N.A.	N.A.	N.A.	14.740	0.718	1.400	N.A.	N.A.	N.A.

https://doi.org/10.5194/egusphere-2025-1370
Preprint. Discussion started: 3 April 2025

BpCr95-3(99)	N.A.	N.A.	N.A.	15.340	0.818	1.400	N.A.	N.A.	N.A.
BPCR96-10	N.A.	N.A.	N.A.	15.940	0.998	2.000	N.A.	N.A.	N.A.
BPCR96-11	N.A.	N.A.	N.A.	14.040	0.715	1.400	N.A.	N.A.	N.A.
BpCr95B-1(99)	N.A.	N.A.	N.A.	16.240	0.877	1.400	N.A.	N.A.	N.A.
BpCR97-3	*N.A.*	*N.A.*	*N.A.*	*17.640*	*0.973*	*1.400*	*N.A.*	*N.A.*	*N.A.*
BpCR97-4	N.A.	N.A.	N.A.	17.540	0.964	1.700	N.A.	N.A.	N.A.
BpCR97-2	*N.A.*	*N.A.*	*N.A.*	*11.940*	*0.757*	*1.000*	*N.A.*	*N.A.*	*N.A.*
BpCR97-1a	N.A.	N.A.	N.A.	16.440	0.906	1.300	N.A.	N.A.	N.A.
BpCR97-1b	N.A.	N.A.	N.A.	16.540	0.876	1.300	N.A.	N.A.	N.A.
BpCr96-21	N.A.	N.A.	N.A.	14.940	0.765	1.100	N.A.	N.A.	N.A.
BpCr96-22	N.A.	N.A.	N.A.	15.840	1.612	1.800	N.A.	N.A.	N.A.
BpCr95-2(99)	N.A.	N.A.	N.A.	15.540	0.784	1.200	N.A.	N.A.	N.A.
Humphreys Basin (HB)									
HB97-1	N.A.	N.A.	N.A.	15.940	0.868	1.200	N.A.	N.A.	N.A.
HB97-2	N.A.	N.A.	N.A.	17.340	0.849	1.300	N.A.	N.A.	N.A.
HB97-3	N.A.	N.A.	N.A.	16.040	0.685	1.100	N.A.	N.A.	N.A.
HB97-4	N.A.	N.A.	N.A.	15.340	0.727	1.400	N.A.	N.A.	N.A.
HB97-5	N.A.	N.A.	N.A.	16.440	0.814	1.300	N.A.	N.A.	N.A.

502

https://doi.org/10.5194/egusphere-2025-1370
Preprint. Discussion started: 3 April 2025

Table 2. Mean surface-exposure age and standard deviation for each sampling location. Location abbreviations: TLC – Top of Lyell Canyon; MLC – Middle elevation within Lyell Canyon; BLC – Bottom of Lyell Canyon; TM-LC – an unnamed roche moutonnée near the junction of Lyell Canyon with Tuolumne Meadows; PD – Pothole Dome; LM – lower Tuolumne Meadows; LD – Lembert Dome; uppMC – Pioneer Basin and the upper reaches of Mono Creek Canyon; midMC – mid-valley location within Mono Creek Canyon; lowMC – the lower reaches of Mono Creek Canyon; LEMinner – the innermost moraine beneath Lake Edison; LEMouter – the outermost moraine beneath Lake Edison; T4m – the Tioga 4 moraine in the Middle Fork of Bishop Creek Canyon; SB&O – scattered boulders and outcrops between the Tioga 4 moraine and the Recess Peak moraines; and HB – Humphrey's Basin.

			Balco et al. (2008) v. 3.0.2 (with 3 Mar 2024 constants)			Marrero et al. (2016) CRONUScalc 2.0			Martin et al. (2017) CREp (on 3 Mar 2024)		
Sampling location	n_i	n_f	Age (ka)	1 σ internal (ka)	1 σ external (ka)	Age (ka)	1 σ internal (ka)	1 σ external (ka)	Age (ka)	1 σ internal (ka)	1 σ external (ka)
Tuolumne Meadows and Lyell Canyon											
TLC	3	3	14.954	0.421	1.572	15.807	0.493	1.303	15.778	0.483	1.663
MLC	1	0	NA	NA	NA	NA	NA	NA	NA	NA	NA
BLC	6	6	14.389	0.220	0.723	15.140	0.200	0.548	15.120	0.206	0.667
TM-LC	1	0	NA	NA	NA	NA	NA	NA	NA	NA	NA
PD	3	2	14.906	0.802	2.717	15.790	0.919	2.438	15.691	0.870	2.981
LM	1	1	15.207	0.239	0.936	16.040	0.434	1.300	15.996	0.230	0.860
LD	3	3	14.686	0.646	2.261	15.507	0.666	1.983	15.463	0.666	2.158
Lake Edison and Mono Creek Canyon											
uppMC	5	5	14.809	0.127	0.448	15.620	0.179	0.521	15.598	0.158	0.498
midMC	2	0	NA	NA	NA	NA	NA	NA	NA	NA	NA
lowMC	1	1	15.137	0.434	1.009	16.040	0.570	1.400	15.997	0.420	0.920
LEMinner	2	2	15.591	0.081	0.223	16.540	0.141	0.344	16.466	0.085	0.222
LEMouter	3	2	19.003	0.593	2.008	19.940	0.566	1.513	19.949	0.601	1.920
Bishop Creek Canyon and vicinity											
T4m	5	5	NA	NA	NA	16.280	0.907	1.646	NA	NA	NA
SB&O	16	14	NA	NA	NA	15.926	0.973	1.565	NA	NA	NA
HB	5	5	NA	NA	NA	16.220	0.740	1.190	NA	NA	NA

https://doi.org/10.5194/egusphere-2025-1370
Preprint. Discussion started: 3 April 2025

4.2. *New ^{10}Be dates from Lake Thomas A. Edison and Mono Creek Canyon*

We report thirteen new ^{10}Be samples from Lake Edison and Mono Creek Canyon. After rejecting three outliers (Sect. S.7.), the ten remaining samples yield ages ranging 19.4–14.7 ka (Version 3 calculator), 20.3–15.4 ka (CRONUScalc 2.0), and 20.4–15.4 ka (CREp; Table 1).

The mean age of the outermost Lake Edison moraine varies by 0.9 kyr (5 %) across the three calculators (Table 2): the Version 3 calculator dates stabilization of the outermost moraine to 19.0 ± 0.6 ka (mean and standard deviation; n = 2; Fig. 4c) while CRONUScalc dates it to 19.9 ± 0.6 ka (Fig. 4d) and CREp dates it to 19.9 ± 0.7 ka (Fig. 4e).

Likewise, the innermost Lake Edison moraine's age also varies by ca. 1 kyr across the calculators (Table 2): the Version 3 calculator suggests stabilization at 15.6 ± 0.1 ka (mean and standard deviation; n = 2; Fig. 4c) while CRONUScalc and CREp place it at 16.5 ± 0.2 ka (Fig. 4d) and 16.5 ± 0.1 ka (Fig. 4e), respectively. Thus, despite calculator-based differences of 0.9 kyr (6 %) in the timing of this event, all three calculators indicate that the outermost Lake Edison moraine predates the onset of rapid deglaciation in the Mono Creek drainage basin by ca. 3.4 kyr, with the Version 3 calculator producing a median estimate of 3.4 kyr (and with a 95 % confidence range of 2.2–4.6 kyr), CRONUScalc producing a median estimate of 3.4 kyr (2.2–4.5 kyr), and CREp producing a median estimate of 3.5 kyr (2.3–4.7 kyr).

Following abandonment of the innermost Lake Edison moraine (i.e., the start of the Tioga 4 deglaciation), the ice-margin retreated up Mono Creek Canyon. A single sample from lower Mono Creek Canyon (lowMC), 7 km behind the innermost Lake Edison moraine and 15 km from the cirque headwall in Pioneer Basin, yields exposure ages of 15.1 ± 0.5 ka (1 σ internal; Version 3; Fig. 4c), 16.0 ± 0.6 ka (CRONUScalc; Fig. 4d), and 16.0 ± 0.5 ka (CREp; Fig. 4e; Table 2). The five samples from upper Mono Creek Canyon (1–5 km from the cirque headwall)

https://doi.org/10.5194/egusphere-2025-1370
Preprint. Discussion started: 3 April 2025

produce mean ages and standard deviations of 14.8 ± 0.2 ka (the Version 3 calculator; Fig. 4c), 15.6 ± 0.2 ka (CRONUScalc; Fig. 4d), and 15.6 ± 0.2 ka (CREp; Fig. 4e; Table 2). All three calculators produce similar median estimates for the duration of the Tioga 4 deglaciation in Mono Creek Canyon (Fig. 4i–k): 0.8 kyr (with a 95 % confidence interval of 0.5–1.1 kyr; the Version 3 calculator), 1.0 kyr (0.5–1.4 kyr; CRONUScalc 2.0), and 0.9 kyr (0.6–1.2 kyr; CREp).

https://doi.org/10.5194/egusphere-2025-1370
Preprint. Discussion started: 3 April 2025

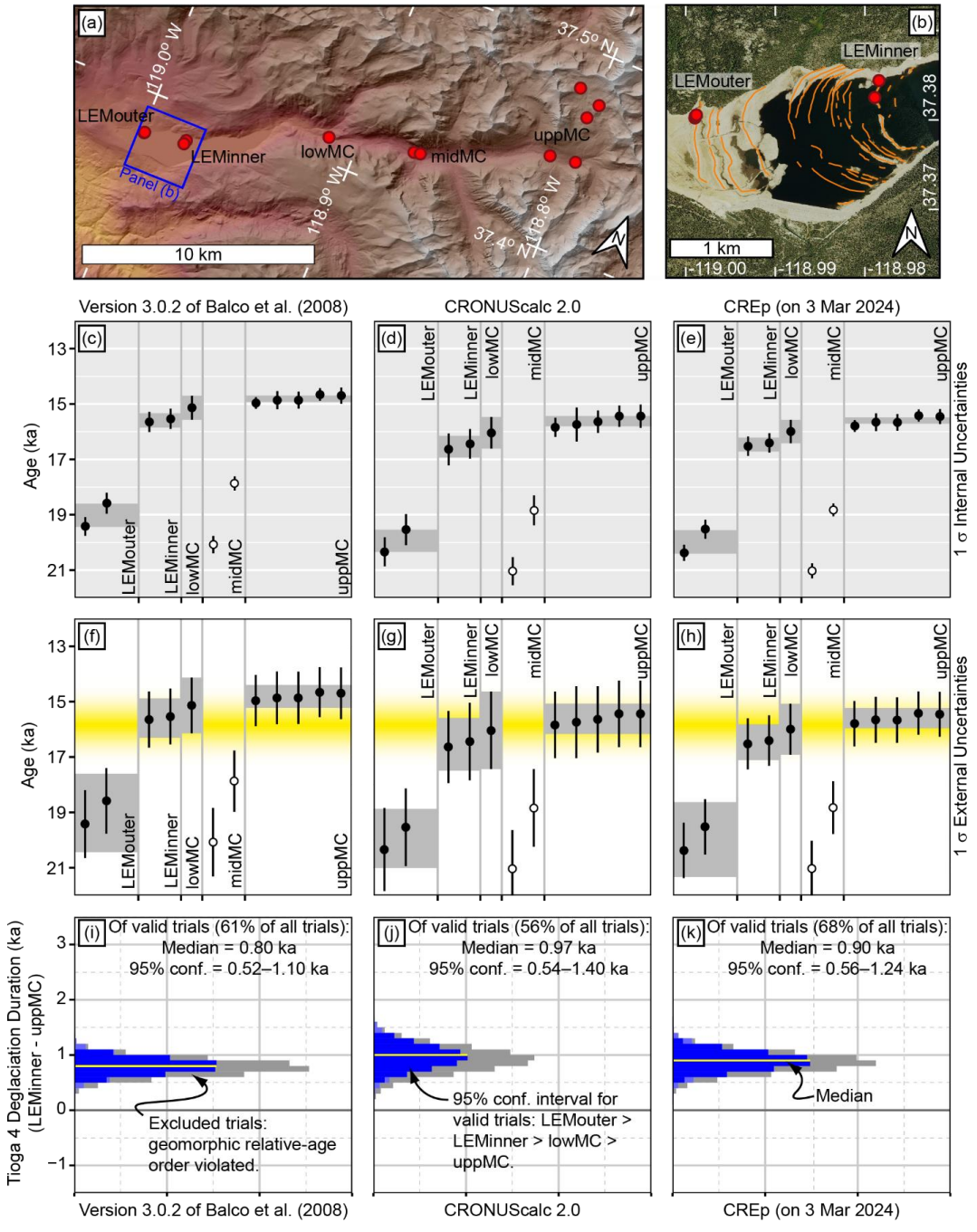

Figure 4. (a) Sampling locations in the Lake Edison and Mono Creek Canyon field area. Sampling-location abbreviations (from distal to proximal): LEMouter – the outermost moraine of the Lake Edison moraine complex; LEMinner – the innermost Lake Edison moraine; lowMC –

https://doi.org/10.5194/egusphere-2025-1370
Preprint. Discussion started: 3 April 2025

lower Mono Creek Canyon; midMC – middle Mono Creek Canyon; and uppMC – upper Mono Creek Canyon. **(b)** 2014 aerial photo of Lake Edison at a low-water stage with moraine crests traced in orange. **(c–e)** Beryllium-10 ages and 1 σ internal uncertainties from the Version 3 Calculator **(c)**, CRONUScalc 2.0 **(d)**, and CREp **(e)**. Gray boxes enclose each sample group's mean age plus/minus one standard deviation. Rejected outliers shown with hollow symbols. Note the extreme outlier (ca. 5 ka) from the outermost Lake Edison moraine (LEM-14-29) is outside the displayed age range. **(f–h)** Beryllium-10 ages and 1 σ external uncertainties. The yellow shading's intensity is proportional to the relative probability of deglaciation, per Phillip's (2016) interpretation of basal radiocarbon dates. **(i–k)** Results of a 1 x 10^5 trial Monte Carlo simulation of deglaciation's duration in this drainage basin. We defined "valid" trials as those where the simulated deglaciation ages run from oldest to youngest in the following order: the outermost Lake Edison moraine, the innermost Lake Edison moraine, lower Mono Creek Canyon, and upper Mono Creek Canyon.

https://doi.org/10.5194/egusphere-2025-1370
Preprint. Discussion started: 3 April 2025

4.3. *Recalculated ^{36}Cl dates from the vicinity of Bishop Creek Canyon*

We report twenty-six recalculated ^{36}Cl ages from the vicinity of Bishop Creek Canyon. The five boulders from the Tioga 4 moraine within the Middle Fork of Bishop Creek Canyon produce a mean age of 16.3 ± 1.7 ka (1 σ external uncertainty), fourteen samples (we reject two samples as outliers; Sect. S.7.) from boulders and bedrock outcrops scattered between the Tioga 4 and Recess Peak moraines (which we will henceforth refer to as the "valley-bottom samples" for brevity) produce a mean age and standard deviation of 15.9 ± 1.6 ka, and the five boulders from Humphreys Basin produce a weighted-mean age of 16.2 ± 1.2 ka (Fig. 5c; Table 2).

Using these mean ages and their associated 1 σ internal uncertainties as input into a Monte Carlo model that requires Tioga 4 moraine abandonment (and stabilization) to precede deglaciation of Humphreys Basin and the valley-bottom locations results in 61 % of the Monte Carlo trials being retained and produces a median estimate for the duration of the Tioga 4 deglaciation within Bishop Creek Canyon of 1.3 kyr with a 95 % confidence range of 0.1–3.3 kyr (Fig. 5d).

https://doi.org/10.5194/egusphere-2025-1370
Preprint. Discussion started: 3 April 2025

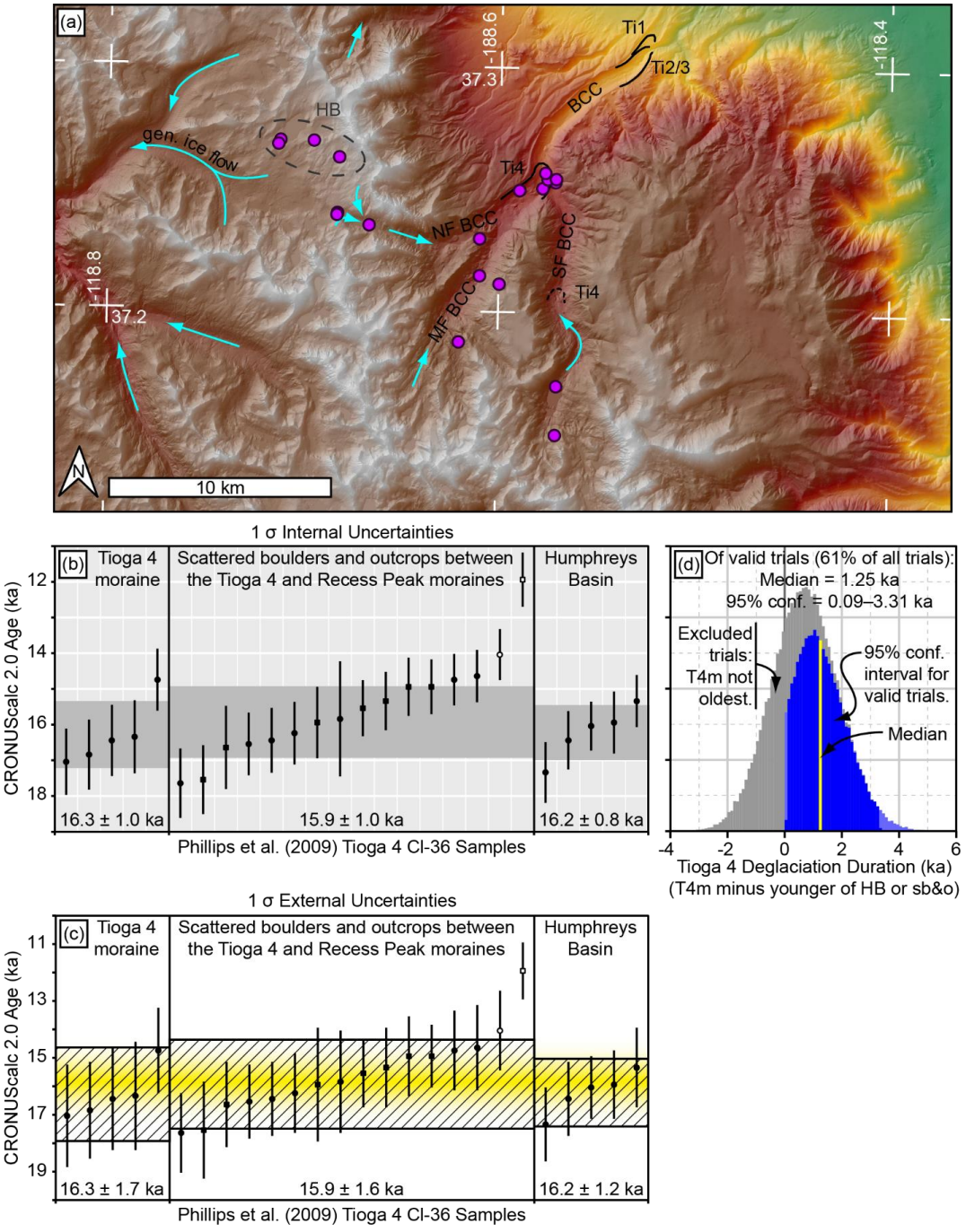

Figure 5. Phillips et al. (2009) Tioga 4 sampling locations in Bishop Creek Canyon and its vicinity, along with the recalculated surface-exposure ages and inferred deglaciation durations.

https://doi.org/10.5194/egusphere-2025-1370
Preprint. Discussion started: 3 April 2025

(a) Phillips et al. (2009) Tioga-4 sampling locations (purple circles). Abbreviations: Ti1 – the Tioga 1 moraine; Ti2/3 – the Tioga 2/3 moraine; Ti4 – the Tioga 4 moraine; HB – Humphrey's Basin; BCC – Bishop Creek Canyon; NF BCC – the North Fork of Bishop Creek Canyon; MF BCC – the Middle Fork of Bishop Creek Canyon; SF BCC – the South Fork of Bishop Creek Canyon. Solid black lines are moraines; the dashed black line is a likely (Tioga 4) ice-marginal position (Phillips et al., 2009). **(b)** Chlorine-36 surface-exposure ages and 1 σ internal age uncertainties. Circles are boulder samples; squares are bedrock samples. Solid symbols are retained samples; hollow symbols are rejected outliers. The gray boxes are the mean age of the retained ^{36}Cl ages plus/minus one standard deviation. **(c)** Chlorine-36 ages and 1 σ external age uncertainties. The hatched boxes enclose the mean age of each sampling group, plus/minus one standard deviation. The yellow shading's intensity is proportional to deglaciation's relative probability, according to Phillip's (2016) interpretation. **(d)** The distribution of Tioga 4 deglaciation durations in the vicinity of Bishop Creek Canyon, based on a 1 x 10^5 trial Monte Carlo simulation. We define "valid" trials as those where the Tioga 4 moraine has the oldest simulated deglaciation age and deglaciation's duration as the time difference between the Tioga 4 moraine's stabilization and the youngest deglaciation age from the other two sampling groups.

https://doi.org/10.5194/egusphere-2025-1370
Preprint. Discussion started: 3 April 2025

4.4. *Updated chronologies for previously published datasets*

Revising the age-depth model for the Swamp Lake paleoenvironmental reconstruction from one based on linear interpolation between adjacent radiocarbon dates to one that permits sedimentation rates to vary throughout the core suggests that age uncertainties on the core's undated horizons are ~2–3 times larger than the age uncertainties on the calibrated radiocarbon dates. Although these age uncertainties vary with core-depth distance to the nearest radiocarbon date, representative 1 σ uncertainties for the undated horizons in the Swamp Lake core of greatest relevance to the Tioga 4 deglaciation are ca. 0.40 kyr verses ca. 0.15 kyr for the radiocarbon dates themselves (Fig. S23; Table S7). Note that – despite updating Swamp Lake's age-depth model from IntCal04 (Reimer et al., 2004) to IntCal20 (Reimer et al., 2020) – the median age estimates for the radiocarbon dates in Swamp Lake's age-depth model are only slightly changed (≤0.15 kyr) from the values reported by Street et al. (2012); the advantage of the new age-depth model that we report here for this core is in the better representing the true dating uncertainties.

With regards to the radiocarbon constraints on the timing of Great Basin lake highstands, updating the various radiocarbon calibrations previously used [i.e., IntCal09 (Reimer et al., 2009) and IntCal13 (Reimer et al., 2013)] to IntCal20 (Reimer et al., 2020) results in new calibrated ages ranging from 0.4 kyr younger to 0.3 kyr older than the ages reported by Munroe and Laabs (2013) and Ibarra et al. (2014), with a mean adjustment of 0.1 kyr younger (Fig. S24; Table S8).

Finally, for the paleoenvironmental reconstruction from McLean's Cave, the median age estimate in Bchron's age-depth model for the various measurement depths in speleothem ML1 ranges from 0.147 kyr younger than the ages reported by Oster et al. (2015) to 0.731 kyr older,

https://doi.org/10.5194/egusphere-2025-1370
Preprint. Discussion started: 3 April 2025

with a mean difference of essentially zero (0.047 kyr older; Figs. S25–S26; Table S9). For the portion of the speleothem with the greatest relevance to this manuscript [sampling depths 132.00–141.85 mm, with ^{230}Th/U dates of 15.433 ± 0.065 ka (1 σ uncertainty) and 16.718 ± 0.159 ka at those depths, respectively (Oster et al., 2015)], the Bchron age-depth model has median ages that are 0.110–0.510 kyr older than the ages reported by Oster et al. (2015), with a mean difference of 0.325 kyr. Bchron's 1 σ age uncertainties for the undated horizons over this sampling-depth interval range from ±0.066 kyr (at the interval's younger, shallower end) to ±0.156 kyr (at the interval's older, deeper end).

5. Discussion

This manuscript's goal is to place the Sierra Nevada's final deglaciation in a robust regional and global context. That narrative, however, depends upon the cosmogenic dates and the three calculators produce exposure ages that disagree by ~5 % (ca. 1 kyr) despite identical inputs. Thus, this discussion is structured as follows. First, we compare the calculated ages for each calculator and document their differences (and similarities). Second, we use the radiocarbon constraints on the timing of the Tioga 4 deglaciation to assess the accuracy of the calculators for these particular ^{10}Be and ^{36}Cl samples. Then, after adopting a preferred set of exposure ages, we return to this manuscript's primary focus and discuss the final deglaciation of the Sierra Nevada within a regional and global context.

5.1. Comparison of the cosmogenic surface-exposure-age calculators

For the thirty-one new ^{10}Be samples presented here, CRONUScalc 2.0 and CREp (on 3 Mar 2024) generated surface-exposure ages that were ~5 % older than those produced by the Version 3 calculator (Fig. 6). In particular, the CRONUScalc ages averaged 5.4 % older (range: 3.2–6.3 %) and the CREp ages averaged 5.3 % older (range: 4.7–5.7 %). These differences

https://doi.org/10.5194/egusphere-2025-1370
Preprint. Discussion started: 3 April 2025

exceed the relative uncertainty in the ^{10}Be concentrations of the samples, which average 1.8 %, and range 1.3–4.4 % (Table S3). Additionally, the age differences between the CRONUScalc 2.0 and the Version 3 calculator results are larger than their combined internal age uncertainties for twenty-six of the thirty-one ^{10}Be samples (84 %); likewise, the age differences between the results from CREp and the Version 3 calculator are larger than their combined internal age uncertainties for thirty of the samples (97 %). Thus, by these measures, the age differences returned by the calculators are significant.

This ~5 % age difference cannot be explained by the scaling or atmospheric models, as all three calculators used LSDn scaling (Lifton et al., 2014) and the ERA-40 atmospheric reanalysis (Uppala et al., 2005), and the ~5 % age difference also cannot be explained by the calculators using different geomagnetic-field reconstructions and ^{10}Be-production-rate-calibration datasets. Although the geomagnetic-field reconstruction is not constant across the calculators, two lines of evidence suggest this variability is not the source of the ~5 % age difference: First, the ages from the Version 3 calculator and CREp were both calculated with the Lifton (2016) geomagnetic reconstruction, and yet the two sets of ages differ by ~5 %. Second, recalculating the exposure ages of these thirty-one samples in CREp (the only calculator of the three that readily enables users to select their preferred geomagnetic reconstruction) with the Lifton et al. (2014) reconstruction (which is used by CRONUScalc) changes the CREp exposure ages by <1 % on average (Table S10). Both the Version 3 calculator and CRONUScalc 2.0 used the CRONUS-Earth primary ^{10}Be-calibration dataset, so the dataset used to calibrate the ^{10}Be production rate also cannot be the reason for the ~5 % age difference across the calculators. Lastly, we note that the corrections for topographic and snow shielding are not particularly large (ranging from 1−14 %), nor are the erosion rates we infer for these samples (≤1 mm yr^{-1}) – and,

https://doi.org/10.5194/egusphere-2025-1370
Preprint. Discussion started: 3 April 2025

in any event, these corrections are a constant for any particular sample across the three calculators. Thus, the ~5 % age difference between the calculators cannot be explained by scaling model, the atmospheric and magnetic reconstructions, the choice of calibration dataset, or particulars about the samples (i.e., topographic shielding, snow shielding, or erosion rate).

We hypothesize that the ~5 % age difference is the result of the calculators using different algorithms for converting a suite of calibration samples into a single value (be it a non-dimensional LSDn scaling factor or a SLHL production rate) for scaling to other locations. Unfortunately, assessing this hypothesis is hindered by the Version 3 calculator reporting a LSDn scaling factor (and not also a SLHL ^{10}Be production rate) and CRONUScalc 2.0 and CREp reporting SLHL production rates (and not also LSDn scaling factors). Fortunately, determining why the calculators are returning different surface-exposure ages is not essential to this paper's purpose. Instead, we focus on two tasks: (1) assessing which calculator is more likely producing more accurate ages for the samples in the dataset reported here; and then (2) placing these dates within the context of previous paleoclimate research.

https://doi.org/10.5194/egusphere-2025-1370
Preprint. Discussion started: 3 April 2025

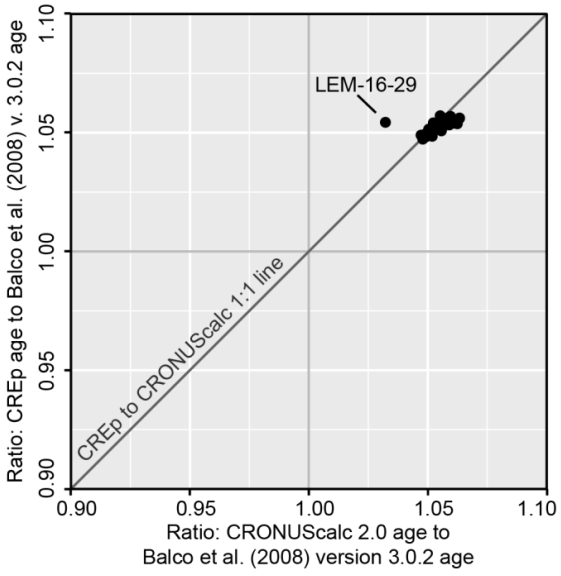

675

676 **Figure 6.** Comparison of the ^{10}Be ages from the three calculators. The Version 3 calculator
677 produces exposure dates that are ~5% younger than the ages produced by CRONUScalc 2.0 and
678 CREp for the thirty-one ^{10}Be samples in this dataset. The outlier is the ca. 5 ka boulder from
679 Lake Edison, which is ca. 9–19 kyr younger than the other samples.
680
681 *5.2 Assessment of the cosmogenic surface-exposure-age calculators*

682 If we accept the interpretation that Tuolumne Meadows deglaciated before 15.4 ka (as
683 suggested by the Greenstone Lake radiocarbon date; Fig. S2; Clark et al., 2003) and that the
684 high-elevation lake basins of the Sierra Nevada deglaciated at 15.75 ± 0.5 ka (Phillips, 2016), as
685 suggested by the bulk-organic radiocarbon dates (Sect. 2.2.2), then the probability distributions
686 on the cosmogenic surface-exposure dates suggest that the CRONUScalc 2.0 and CREp dates are
687 probably more accurate than the dates from the Version 3 calculator for the limited range of
688 elevations (2300–3500 m), latitudes (37–38° N), longitudes (118–120° W), and ^{10}Be
689 concentrations (3–6 x 10^5 atoms g^{-1}) represented by the thirty-one ^{10}Be samples in this
690 manuscript's dataset (Figs. 3e–g and 4f–h). We emphasize this assessment is (1) probabilistic
691 and (2) predicated on the accuracy of the bulk-sediment radiocarbon dates. Because bulk-

https://doi.org/10.5194/egusphere-2025-1370
Preprint. Discussion started: 3 April 2025

sediment radiocarbon dates can be biased toward older ages by the presence of inorganic "dead" carbon, we first assess the possibility that these bulk-sediment radiocarbon dates from the Sierra Nevada are contaminated with radioactively dead carbon (Sect. 5.2.1.) before returning to the topic of the surface-exposure calculators and their relative accuracy for the Tioga 4 deglaciation in the Sierra Nevada (Sect. 5.2.2.).

5.2.1 On the accuracy of the bulk-organic radiocarbon dates

Bulk-organic radiocarbon dates are problematic for accurate chronologies because trace amounts of inorganic carbon, if present in the sediments, will bias the radiocarbon dates toward older ages due to the "hardwater effect" (Godwin, 1951, p. 306; Deevey et al., 1954; Oana and Deevey, 1960; Philippsen, 2013). However, three lines of evidence suggest dead carbon is not a significant concern for these samples. First, carbonate bedrock is absent within the radiocarbon-dated drainage basins; instead, these watersheds are etched into the granitic rocks of the Sierra Nevada (Bateman and Wones, 1972; Bateman et al., 1983; Huber, 1983).

Second, Clark and Gillespie (1997) tested for dead carbon in four other granitic watersheds of the Sierra Nevada by dating macrofossils (twigs, branches, and charcoal) and directly adjacent bulk sediment (organic silt, gyttja, and peat) in four cores. In four of five cases, these paired radiocarbon dates agree within 1 σ. In the case of the exception, the bulk sediment (gyttja) is ca. 1.1 kyr older than the macrofossil, which was a piece from a "large" branch. While this age offset could be explained by 10 % of the carbon in the gyttja being dead with respect to ^{14}C activity, Clark and Gillespie (1997) rejected this interpretation because – crucially – one of the four other radiocarbon-dated pairs in their dataset came from the same sediment core (BL-2, from Upper Baboon Lake in the Bishop Creek drainage basin; Fig. 1f) and the macrofossil and bulk-sediment in this other radiocarbon-date pair had indistinguishable ages: the macrofossil

https://doi.org/10.5194/egusphere-2025-1370
Preprint. Discussion started: 3 April 2025

(twig) dated to 7,900 ± 60 ^{14}C-yrs and the bulk sediment (gyttja) dated to 7,890 ± 60 ^{14}C-yrs. Therefore, Clark and Gillespie (1997) interpreted the mismatched radiocarbon-date pair as resulting from the large branch sinking into then-flocculent gyttja when it landed in the pond – a phenomenon observable within modern ponds and interpreted for other lacustrine cores (e.g., Davis et al., 2019, Fig. 16) – and we accept their interpretation for the observed age offset in this pair of radiocarbon dates.

Finally, Swamp Lake also occupies a granitic watershed within the Sierra Nevada and all thirteen radiocarbon dates in its age-depth model were on bulk sediment; Street et al. (2012) tested the core's sediments for carbonates by fumigating samples with concentrated HCl and comparing them with unfumigated samples. Street et al. (2012) found no detectable carbonates within the Swamp Lake core.

Although a lack of compelling evidence for dead carbon within the lacustrine sediments of five granitic watersheds in the Sierra Nevada [i.e., Swamp Lake plus the four investigated by Clark and Gillespie (1997)] does not preclude its presence in the sediments of other granitic watersheds in the Sierra Nevada, there is no evidence for dead carbon in the lacustrine sediments of the Sierra Nevada's granitic watersheds. Therefore, we accept the bulk-organic radiocarbon dates reviewed in Sect. 2.2.2 as accurate minimum limits on the timing of the Tioga 4 deglaciation.

5.2.2. On the accuracy of the cosmogenic surface-exposure-age calculators

Accepting the bulk-organic radiocarbon dates as accurate minimum limits on the timing of the Tioga 4 deglaciation suggests that the CRONUScalc and CREp dates are probably more accurate than the Version 3 calculator's dates for the ^{10}Be samples reported here. Our argument is as follows: After excluding outliers, nine sampling locations remain (Table 2). For six of these

https://doi.org/10.5194/egusphere-2025-1370
Preprint. Discussion started: 3 April 2025

nine locations (lower Tuolumne Meadows, Pothole Dome, Lembert Dome, the top of Lyell Canyon, lower Mono Creek Canyon, and upper Mono Creek Canyon), the CRONUScalc and CREp dates produce mean sampling group ages closely bracketing 15.75 ka (≤0.3 kyr). These mean ages range from 16.0–15.5 ka (Table 2). For the three remaining locations, larger deviations from 15.75 ka seem reasonable. These three exceptions are (from oldest to youngest): (1) the outermost moraine beneath Lake Edison (which predates the innermost Lake Edison moraine by ca. 3.4 kyr across all three calculators; Fig. 4c–e); (2) the innermost moraine beneath Lake Edison, which records the start of the Tioga 4 deglaciation, and not the deglaciation of high-elevation lake basins, as the radiocarbon dates do; and (3) the bottom of Lyell Canyon, which has comparatively young exposure ages across all three calculators and likely hosted a substantially greater Tioga 4 ice thickness than the radiocarbon-dated lake basins (Wahrhaftig et al., 2019).

In contrast to CRONUScalc and CREp, the Version 3 calculator produces mean ages that are 0.5–1.1 kyr younger than 15.75 ka for the six locations mentioned above (Figs. 3e and 4f). These mean ages range from 15.2–14.7 ka (Table 2). Likewise, within this set of results, the innermost Lake Edison moraine likely stabilized ca. 0.1–0.5 kyr after the start of organic accumulation in the high basins of the Sierra Nevada. Additionally, the Version 3 calculator's exposure ages from locations analogous to the radiocarbon-dated lake basins [such as the top of Lyell Canyon (with a mean age of 15.0 ka) and the upper reaches of Mono Creek Canyon (14.8 ka)] postdate the high-elevation lake-basin radiocarbon dates by ca. 0.9 kyr (Figs. 3e and 4f). Shifting the bulk-organic radiocarbon ages 0.9 kyr younger, into agreement with the most probably ages from the Version 3 calculator, would require 7–11 % of the carbon in the sediments of Highlands, Greenstone, and East Lakes be "dead" with respect to ^{14}C activity.

https://doi.org/10.5194/egusphere-2025-1370
Preprint. Discussion started: 3 April 2025

Considering Tuolumne Meadows in particular, where the radiocarbon-dated deglacial chronology is the strongest of all our field areas, CRONUScalc and CREp produce mean deglaciation ages of 16.0–15.5 ka for lower Tuolumne Meadow, Pothole Dome, and Lembert Dome – while the Version 3 calculator produces mean ages of 15.2–14.7 ka (Table 2). In comparison, Greenstone Lake was both deglaciated and accumulating organic carbon by 15.4 ka (Fig. S2; Sect. 2.2.2) – and Greenstone Lake was ≤4 km from the accumulation zone that fed ice into Tuolumne Meadows (Huber, 2007; Wahrhaftig et al., 2019). If Greenstone Lake was deglaciated and accumulating organic carbon by 15.4 ka, then it seems likely that our sampling sites in lower Tuolumne Meadows (~30 m above the modern floor of Tuolumne Meadows) and on Pothole Dome (~70 m) and Lembert Dome (~230 m) were also deglaciated by that time.

We tested whether recalculating the ^{10}Be surface-exposure ages with the most precisely determined ^{10}Be production rate from western North America (the Promontory Point production rate; Lifton et al., 2015) would shift the ages older – and thus bring the results of the Version 3 calculator into better agreement with the radiocarbon dates from the Sierra Nevada (Fig. S2). We instead find that the Lifton et al. (2015) calibration dataset results in even younger exposure ages (Table S11). Therefore, with the evidence available to us, we conclude that the Version 3 calculator is probably producing exposure ages that are ~5 % too young for the thirty-one ^{10}Be samples in this location and that the CRONUScalc and CREp dates are more consistent with the current radiocarbon chronology.

Accordingly, with the goal of streamlining the Discussion going forward, we will henceforth exclusively refer to the CRONUScalc 2.0 ages, which are indistinguishable from the CREp ages. This interpretive decision results in the following deglacial narrative: the innermost Lake Edison moraine stabilized a few hundred years prior to the start of organic accumulation in

https://doi.org/10.5194/egusphere-2025-1370
Preprint. Discussion started: 3 April 2025

the high-elevation ponds of the Sierra Nevada (Fig. 4g), the six sampling locations mentioned above were then exposed to cosmic rays around the same time that the ponds began accumulating organic carbon, and deglaciation concluded with the melting of the valley-bottom ice remnants, where Tioga 4 ice thicknesses were the greatest (e.g., the bottom of Lyell Canyon; Figs. 3f). This narrative is consistent with geomorphic interpretations of rapid deglaciation and ice thinning in the Sierra Nevada at the end of the last glaciation (Clark, 1976; Clark and Clark, 1995) and with observations from Alaska (Cushing, 1891; Reid, 1896; Field, 1947; Mickelson, 1971; Syverson, 1995), and interpretations (Goldthwait, 1938; Lowell, 1985; Lowell et al., 1990) and dating (Bierman et al., 2015; Davis et al., 2015; Koester et al., 2017, 2021; Corbett et al., 2019; Drebber et al., 2023; Halsted et al., 2024) from New England and adjacent regions (Barth et al., 2019) for how rapid deglaciation proceeds in mountainous landscapes (Goldthwait and Mickelson, 1982).

5.3 New ^{10}Be and revised ^{36}Cl constraints on the timing and duration of the Tioga 4 deglaciation

5.3.1. On the timing of the Tioga 4 deglaciation

Within this context, the best direct estimate for the culmination of the Tioga 4 readvance and the start of the Tioga 4 deglaciation is 16.4 ± 0.8 ka (1 σ external; Fig. 7a). This age is the mean and standard deviation of the seven cosmogenic surface-exposure ages from the two Tioga 4 moraines dated by this study: the two ^{10}Be dates from the innermost Lake Edison moraine (which independently dates to 16.5 ± 0.4 ka; Fig. 4g; Table 2) and the five ^{36}Cl dates from the Tioga 4 moraine in Bishop Creek Canyon (which independently dates to 16.2 ± 1.7 ka; Fig. 5c). Although the most distal sampling location in Tuolumne Meadows does not date the start of the

https://doi.org/10.5194/egusphere-2025-1370
Preprint. Discussion started: 3 April 2025

Tioga 4 deglaciation, we note that it also produces an exposure age (16.0 ± 1.3 ka) similar to the stabilization ages of these two innermost moraines.

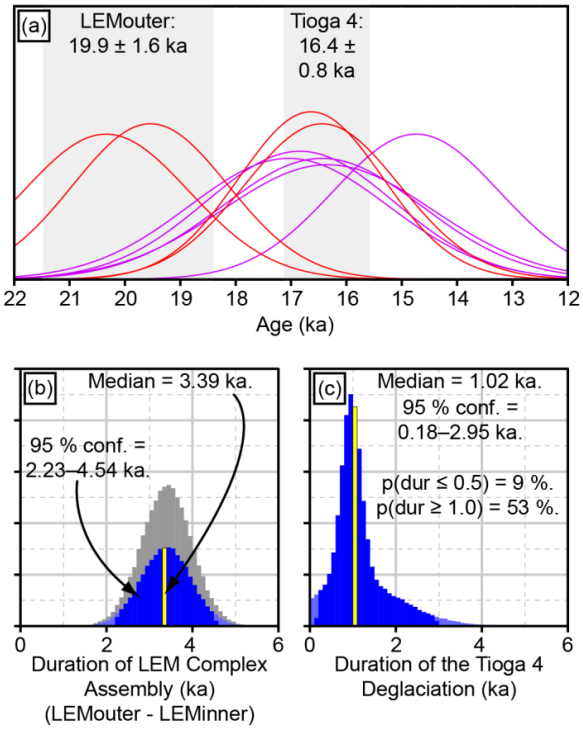

Figure 7. (a) The 68 % confidence (1 σ) ranges for the outermost Lake Edison moraine (LEMouter) and for the start of the Tioga 4 deglaciation (which is dated by two ^{10}Be and five ^{36}Cl dates across two innermost moraines). Red lines are the probability densities of the individual ^{10}Be dates (as calculated by CRONUScalc 2.0) and the purple lines are the same for the ^{36}Cl samples. Samples constraining the end of the Tioga 4 deglaciation (rather than its beginning) are omitted for clarity. **(b)** The inferred duration of moraine construction in the Lake Edison moraine complex. **(c)** Duration of the Tioga 4 deglaciation in 1 x 10^5 Monte Carlo simulations (5 x 10^4 from Mono Creek Canyon and 5 x 10^4 from Bishop Creek Canyon).

Prior to the start of the Tioga 4 deglaciation, regional climate experienced a few thousand years that were at least episodically conducive to moderate glaciation in the Sierra Nevada. This interpretation follows from two observations: first, the 3.4 kyr difference in the mean ages of the outermost and innermost Lake Edison moraines (with a 95% confidence interval of 2.2–4.5 kyr; Fig. 7b); second, the presence of approximately nine additional (undated) end moraines between

https://doi.org/10.5194/egusphere-2025-1370
Preprint. Discussion started: 3 April 2025

these two moraines (Fig. 4b). Although these numerous, closely spaced moraines (~11 in 2 km) are suggestive of glacial advances driven by interannual climate variability (e.g., Anderson et al., 2014; Barth et al., 2017), where stochastic variations in temperature and precipitation are superimposed on a climate that is approximately stable over a longer time, the presence of the Lake Edison moraine complex does not require this interpretation. The moraines might truly represent large-magnitude and long-term variations in summer temperature and winter precipitation in the Sierra Nevada over the ca. 20–16 ka interval. However – regardless of whether the moraines in the Lake Edison complex represent interannual climate variability (i.e., weather), climate change, or some combination thereof – they indicate the former Mono Creek Glacier's ELA dropped to ~2800 m (Phillips, 2016) between ca. 20 ka and ca. 16.5 ka before returning to higher elevations.

5.3.2. On the duration of the Tioga 4 deglaciation

The glaciers of the Sierra Nevada rapidly melted after the start of the Tioga 4 deglaciation at 16.4 ± 0.8 ka; our best estimate for the full duration of the Tioga 4 deglaciation in the central Sierra Nevada from innermost moraine stabilization to the melting of the last remanent ice masses is 1.0 kyr, with a 95 % confidence range of 0.2–3.0 kyr (Fig. 7c).

Although the original analysis of the ^{36}Cl dates from the vicinity of Bishop Creek Canyon concluded that the Tioga 4 deglaciation was probably ≤500 years and certainly <1000 years (Phillips et al., 2009) – we find a ~50 % probability that the full duration of the Tioga 4 deglaciation in the central Sierra Nevada was 1000 years or longer and only a ~10 % probability that it was 500 years or less (Fig. 7c). However, despite finding that the time required for deglaciation was ca. 500 years longer than interpreted by Phillips et al. (2009), the ^{10}Be dates from Lake Edison and Mono Creek Canyon (Fig. 4) support the fundamental conclusion of

https://doi.org/10.5194/egusphere-2025-1370
Preprint. Discussion started: 3 April 2025

Phillips et al. (2009) that the deglacial history of Bishop Creek Canyon and its vicinity (Fig. 5) is representative of other locations within the Sierra Nevada.

Moreover, the new ^{10}Be dates are consistent with the interpretations of multiple researchers (Clark, 1976; Clark and Clark, 1995; Phillips et al., 2009) that the Sierra Nevada's final deglaciation was a geomorphically abrupt event. For instance, the bottom of Lyell Canyon sampling location has the youngest mean surface-exposure age across all the sampling locations reported here (Fig. 3c; Table 2) – and a trimline-based ice-thickness reconstruction (Wahrhaftig et al., 2019) indicates the bottom of Lyell Canyon hosted an ice thickness greater than any other location we sampled. Tioga 4 ice thicknesses over the bottom of Lyell Canyon sampling site (~600 m) were ~2–4x greater than the ice thicknesses over the sampling sites in Tuolumne Meadows (~300 m) and at the top of Lyell Canyon (~150 m). Additionally, ice thicknesses in Lyell Canyon were also ~50 % greater than ice thicknesses over Greenstone Lake (~400 m), thus explaining why the bottom of Lyell Canyon almost certainly (99.4 % probability, per the radiocarbon date's probability-density distribution from Bchron (Haslett and Parnell, 2008) and our Monte Carlo modeling of the surface-exposure ages) deglaciated after the beginning of organic accumulation in Greenstone Lake. The observation that the locations with the thickest ice were the last to deglaciate, regardless of their distance from the cirque headwalls, indicates that the deglaciation was driven by a relatively sudden and large rise in the ELA.

5.4. Geomorphic and climatological constraints on the magnitude of deglacial climate change

Geomorphic and modern climatological observations suggest that this widespread and rapid deglaciation (the Tioga 4 deglaciation) was driven by a summertime warming of ≥2 °C, a wintertime drying of ≥35 %, or some combination thereof. The temperature-change reconstruction is based on the interpretation that the deglaciation was driven by ≥600 m rise in

https://doi.org/10.5194/egusphere-2025-1370
Preprint. Discussion started: 3 April 2025

the ELA (as reviewed in Sect. 2.2.1.) and the observation that modern surface-temperature lapse rates are ~3–4 °C km^{-1} in the higher elevations of the Sierra Nevada and the Cascade Range (Wolfe, 1992). Importantly, the similar lapse rates in both mountain ranges indicate modern high-elevation lapse rates are mostly independent of latitude and we assume a similar independence for the deglaciation period (Ye et al., 2023). Combining the minimum ELA change with the estimated lapse rate suggests the Sierra Nevada's final deglaciation was driven by a summertime warming of ≥2 °C, assuming no change in winter precipitation (Leonard et al., 2023).

Conversely, if we assume no change in summer temperatures and accept a 20 % precipitation decrease as the mass-balance equivalent of a 1 °C warming (Oerlemans, 2005), then the Tioga 4 deglaciation could have alternatively been driven by a 35 % (or greater) reduction in winter precipitation – with intermediate temperature and precipitation combinations possibly, and perhaps likely.

5.5. Constraints from regional paleoclimate proxies on the timing and nature of the climate change that drove the Tioga 4 deglaciation

We examine five paleoclimate records from western North America and adjacent portions of the Pacific Ocean that further illuminate the timing and drivers of the Tioga 4 deglaciation: (1) the lacustrine core from Swamp Lake (~40 km west of Tuolumne Meadows; Fig. 1b; Street et al., 2012), (2) speleothem ML1 from McLean's Cave (~100 km west-northwest of Tuolumne Meadows; Fig. 1b; Oster et al., 2015), (3) twenty-five radiocarbon dates from seventeen Great Basin Pleistocene lakes (Fig. 1a; Munroe and Laabs, 2013; Ibarra et al., 2014), (4) ODP core 893A from the Santa Barbara Basin (Fig. 1a; Hendy et al., 2002), and (5) the MD02-2515 sea-surface temperature (SST) record from the Gulf of California (Fig. 1a;

https://doi.org/10.5194/egusphere-2025-1370
Preprint. Discussion started: 3 April 2025

McClymont et al., 2012). We compare these records with the $\delta^{18}O$ record from Ostolo Cave in Spain, which records the timing of Heinrich Event 1 (Bernal-Wormull et al., 2021; Pérez-Mejías et al., 2021).

5.5.1. Swamp Lake

The paleoenvironmental proxy records from Swamp Lake (Fig. 1a) suggest the central Sierra Nevada warmed at 16.4 ± 0.4 ka and that this warmth persisted for ca. 1.3–1.6 kyr. The magnetic susceptibility of Swamp Lake's sediments decreased more than thirty-fold over a ca. 0.1 kyr interval at 16.4 ± 0.4 ka and remained at near-zero values for ca. 1.6 kyr (Fig. 8a). Simultaneously, the core's total organic carbon (TOC) content started trending higher at 16.5 ± 0.4 ka and increased twenty-fold over ca. 1.3 kyr. Similar trends are recorded in the other proxy records from Swamp Lake, such as: the tripling of the molar ratio of carbon to nitrogen, a nine-fold increase in biogenic silica concentration, and a local $\partial^{13}C$ maxima (Street et al., 2012). These changes reflect the return of sub-alpine conifers and associated terrestrial vegetation in Swamp Lake's small (1.3 km^2) drainage basin, which stabilized soils and allowed a near-order-of-magnitude increase in diatom abundance via decreased turbidity (Street et al., 2012). Upward migration of the upper treeline is usually driven by warming temperatures (e.g., LaMarche and Mooney, 1967; Denton and Karlén, 1977; Kullman, 1986, 1995; Scuderi, 1987). We infer that the Sierra Nevada warmed at 16.4 ± 0.4 ka and that these warmer temperatures lasted for ca. 1.3–1.6 kyr.

https://doi.org/10.5194/egusphere-2025-1370
Preprint. Discussion started: 3 April 2025

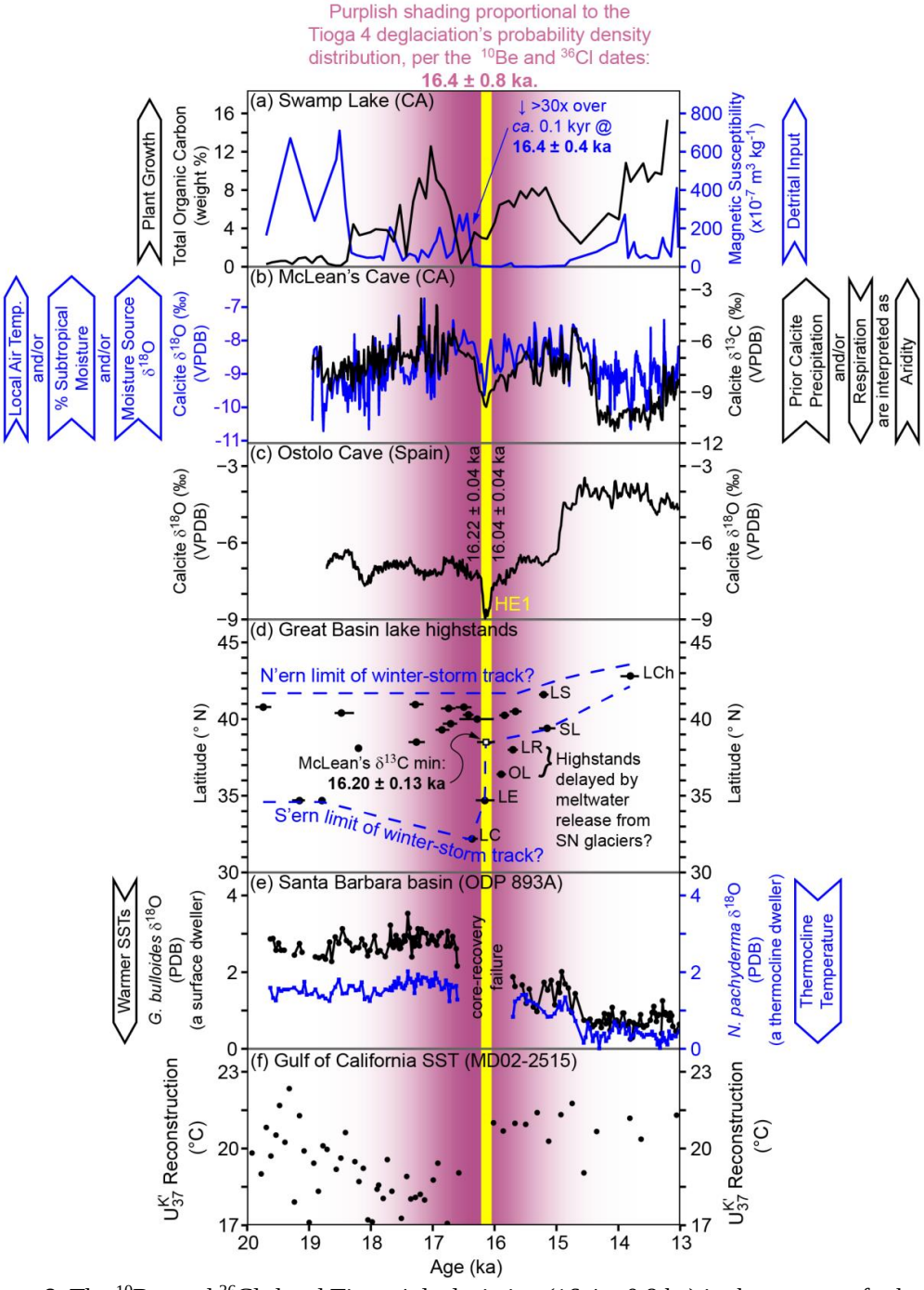

911
912 **Figure 8.** The ^{10}Be- and ^{36}Cl-dated Tioga 4 deglaciation (16.4 ± 0.8 ka) in the context of other
913 paleoclimate records. **(a)** The total organic carbon (TOC) and magnetic susceptibility records
914 from Swamp Lake (~40 km west of Tuolumne Meadows; Street et al., 2012) on the revised age-

https://doi.org/10.5194/egusphere-2025-1370
Preprint. Discussion started: 3 April 2025

depth model that we present here (Sect. S.8.; Fig. S23; Table S7). **(b)** The $\delta^{13}C$ and $\delta^{18}O$ records from McLean's Cave (~100 km west-northwest of Tuolumne Meadows; Oster et al., 2015) on the revised age-depth model that we present here (Sect. S.10.; Fig. S25; Table S9). **(c)** The $\delta^{18}O$ record from speleothem OST2 (Ostolo Cave, Spain), which constrains the start of Heinrich Event 1 to 16.22 ± 0.04 ka and its end to 16.04 ± 0.04 ka (Bernal-Wormull et al., 2021). **(d)** The timings of Great Basin lake highstands (Munroe and Laabs, 2013; Ibarra et al., 2014), as recalculated here (Table S8). **(d)** The *G. bulloides* $\delta^{18}O$ and *N. pachyderma* $\delta^{18}O$ records from ODP core 893A from the Santa Barbara Basin (Hendy et al., 2002); note that lower $\delta^{18}O$ values record warmer temperatures. **(e)** The $U^{K'}_{37}$-index reconstruction of sea-surface temperatures from core MD02-2514 in the Gulf of California; the precision of these temperature estimates is ±0.6 °C (McClymont et al., 2012).

5.5.2. *McLean's Cave*

The $\delta^{13}C$ and $\delta^{18}O$ records from McLean's Cave (Fig. 8b; Oster et al., 2015) suggest the west-central Sierra Nevada warmed and dried between 16.20 ± 0.13 ka and 14.71 ± 0.19 ka. Interestingly, these dates are indistinguishable from the start of Heinrich Event 1 in the North Atlantic (16.22 ± 0.04 ka; Fig. 8c; Bernal-Wormull et al., 2021; Pérez-Mejías et al., 2021) and the start of the Bølling (14.74 ± 0.06 ka; Lemieux-Dudon et al., 2010). The $\delta^{13}C$ record trends higher over that 1.5 kyr interval, driven by increased prior calcite precipitation (PCP) and/or decreased soil respiration, both of which record a drying climate (Oster et al., 2015). The $\delta^{18}O$ record reaches a local minimum nearly contemporaneously with the just mentioned $\delta^{13}C$ minimum (the $\delta^{18}O$ minimum is one isotopic-measurement-interval earlier in the core, at 16.23 ± 0.13 ka) and rises, episodically, for ca. 0.8 ka. The 2.17 ‰ $\delta^{18}O$ increase over that interval might reflect warmer temperatures in the Sierra Nevada (up to 3–4 °C; Rozanski et al., 1993), a ~40% reduction in moisture delivery to the range from the North Pacific (relative to moisture sourced from the subtropics), a change in the $\delta^{18}O$ of the moisture-source regions, or some combination thereof. Thus, the $\delta^{13}C$ record implies drying of the west-central Sierra Nevada starting at 16.20 ± 0.13 ka and the $\delta^{18}O$ record permits both it and warming.

5.5.3. Great Basin lakes

https://doi.org/10.5194/egusphere-2025-1370
Preprint. Discussion started: 3 April 2025

Considering the western United States more broadly, the temporal and spatial pattern of Great Basin lake-level highstands (Fig. 8d) and numerical modeling suggests that these highstands were fed by an invigorated subtropical jet stream and a deeper and southeastward-shifted Aleutian Low, which collectively increased moisture transport into the Great Basin via atmospheric rivers (McClymont et al., 2012; Chiang et al., 2014; McGee et al., 2018). Notably, the southern limit of lake-level highstands shows a ~6° northward jump between ca. 16.4 ka and ca. 16.2 ka, suggesting a major reorganization in atmospheric circulation over western North America at that time (Fig. 8d), coincident with the deglaciation of the Sierra Nevada. In particular, the ~6° northward jump is defined by (1) Lake Cochise (at 32° N; "LC" on Figs. 1a and 8d) abandoning its 1274 m shoreline at 16.37 ± 0.21 ka (Waters, 1989; Munroe and Laabs, 2013), (2) Lake Estancia (at 35° N; "LE" on Figs. 1a and 8d) abandoning its 1890 m shoreline at 16.16 ± 0.15 (Allen and Anderson, 2000; Munroe and Laabs, 2013), and by (3) the abrupt rise in $\delta^{13}C$ in McLean's Cave (at 38° N; Oster et al., 2015) at 16.20 ± 0.13 ka. Note that the highstands of meltwater-fed Owens Lake (at 36° N) and Lake Russell (at 38° N) post-date this atmospheric reorganization due to the release of meltwater from the rapidly melting glaciers of the Sierra Nevada.

5.5.4. The Santa Barbara Basin and the Gulf of California

The interpretation that rapid deglaciation began in the Sierra Nevada at ca. 16.2 ka is also consistent with marine-sediment cores from the Santa Barbara Basin and the Gulf of California. Although the Santa Barbara Basin core (ODP core 893A; Hendy et al., 2002) unfortunately lacks data between ca. 16.6 ka and ca. 15.7 ka due to a core-recovery failure, the average $\delta^{18}O$ value of *G. bulloides* (a surface-dwelling planktonic foraminifera) decreased approximately 1.4 ‰ over this missing interval (Fig. 8e), which is consistent with warming. Changes in the core's

https://doi.org/10.5194/egusphere-2025-1370
Preprint. Discussion started: 3 April 2025

967 planktonic-foraminifera assemblage suggests Santa Barbara Basin SSTs warmed ~5 °C over this
968 missing interval. This large change in SSTs suggests that the Aleutian Low weakened and
969 migrated to the northwest, causing the California Current to weaken (Hendy, 2010), slowing the
970 flow of subpolar water into the basin (Hendy and Kennett, 2000; Hendy et al., 2002).

971 Similarly, the $U^{K'}_{37}$ reconstruction from Gulf of California core MD02-2515 (McClymont
972 et al., 2012) indicates SSTs there warmed 4.0 ± 0.9 °C between 16.8 ka and 16.0 ka (Fig. 8f). A
973 parallel TEX^{H}_{86} reconstruction from the core demonstrates little-to-no warming over this time
974 interval at the thermocline. The divergence in these temperature proxies implies a sharp
975 reduction in upwelling, which in turn suggests a reduction in northwesterly winds over the Gulf
976 of California (Ganeshram and Pedersen, 1998), such as might accompany a northwestward
977 migration of the northwest Pacific's subtropical high (McGee et al., 2018). Such a reorganization
978 in atmospheric circulation would have shutdown upwelling in the Gulf of California and allowed
979 warm, tropical waters to flow into it, producing the warmer SSTs, as is currently observed during
980 Northern Hemisphere spring (Ganeshram and Pedersen, 1998; McClymont et al., 2012).

981 If the magnitudes of these SST warmings in the Santa Barbara Basin and the Gulf of
982 California are also representative of the summer air-temperature change in the central Sierra
983 Nevada, then the warming would have been more than enough to deglaciate the range (Sect.
984 5.4.).

985 5.6. *Hypothesized cause of the Tioga 4 deglaciation*

986 The close correspondence in timing between the start of the Tioga 4 deglaciation in
987 California (16.20 ± 0.13 ka, as indicated by the $\delta^{13}C$ data from McLean's Cave; Fig. 8d) and the
988 start of Heinrich Event 1 in the North Atlantic (16.22 ± 0.04 ka; Fig. 8c) suggests a mechanistic
989 connection between the two events. We hypothesize that Heinrich Event 1 withdrew such a

https://doi.org/10.5194/egusphere-2025-1370
Preprint. Discussion started: 3 April 2025

volume of ice from the Laurentide Ice Sheet (LIS) that atmospheric circulation reorganized over North America in response. As the LIS shrinks and thins, the Aleutian Low weakens and moves northward while the subtropical high in the eastern Pacific strengthens (Bartlein et al., 1998; Otto-Bliesner et al., 2006; Wong et al., 2016; Jones et al., 2018). Also, as the LIS thins, it becomes a less formidable obstacle to atmospheric circulation, which enables the polar jet stream – formerly split by the LIS (Fig. 9a), with a weaker branch passing to the north of the ice sheet and a stronger branch passing to the south (Kutzbach and Wright Jr, 1985; Manabe and Broccoli, 1985; Kutzbach and Guetter, 1986; Bromwich et al., 2004; Löfverström et al., 2014; Lora et al., 2016; Wang et al., 2024) – to reunify (Fig. 9b). We interpret that these changes in the Aleutian Low and the Subtropical High caused the ITCZ to shift northward over the eastern Pacific Ocean, weakening the subtropical jet stream (McGee et al., 2018), reducing the frequency of atmospheric rivers, and causing them to "land" on North America to the north of the central Sierra Nevada (which is at 37–38° N). Based on the timing and latitude of lake-level highstands (Fig. 8d), we interpret this northward shift in the mean latitude of landfalling atmospheric rivers to be ~6°.

Interestingly, the TraCE-21k transient simulation of deglacial climate produced only one major reorganization in atmospheric circulation over North America's west coast during the deglaciation period – and it was a 7° northward shift in the polar jet stream (He et al., 2013; Lora et al., 2016). This northward shift in the polar jet stream was coincident with polar jet reunification and that reunification was triggered by a ~1.4 km thinning of the LIS, with the TraCE-21k model switching from ICE-5G's "15.0 ka" ice-sheet topography to ICE-5G's "14.0 ka" topography (Peltier, 2004) at 13.87 ka in the transient model. Although we interpret deglaciation of the Sierra Nevada as occurring at ca. 16.2 ka and being driven by a northward

https://doi.org/10.5194/egusphere-2025-1370
Preprint. Discussion started: 3 April 2025

expansion of Hadley Cell circulation on the eastern Pacific and a ~6° northward shift in the mean latitude of land-falling atmospheric rivers (and not directly by a northward shift in the polar jet stream), the TraCE-21k model results do underscore the sensitivity of North American atmospheric circulation to LIS thickness and contain a northward shift in atmospheric circulation that is comparable to what we see in the lake-level-highstand data (Fig. 8d).

Supporting evidence for the ca. 16.2 ka deglaciation of the Sierra Nevada being driven by an atmospheric reorganization over North America in response to Heinrich Event 1 comes from the West Antarctica Ice Sheet (WAIS) Divide deuterium record (Jones et al., 2018). This record indicates interannual to decadal climate variability in the high southern latitudes was almost twice as large during the LGM as it was during the Holocene. Jones et al. (2018) link this enhanced variability to the mean location of tropical convection in the Pacific, with a thick LIS causing a deeper and south-shifted Aleutian Low that weakens tropical Pacific winds. The weaker winds then cause the western warm pool to spill eastward, as during modern El Niño events. The enhanced isotopic variability at WAIS Divide comes to an abrupt end at ca. 16 ka, implying a substantial thinning of the LIS at that time and a concomitant reorganization in atmospheric circulation over North America (and the tropical Pacific).

In summary, we infer Heinrich Event 1 sufficiently thinned the LIS at ca. 16.2 ka to trigger an atmospheric reorganization (Fig. 9). That atmospheric reorganization brought drier winters and warmer summers to what is now the southwestern United States. In response, the central and southern Sierra Nevada essentially deglaciated and formerly expansive lakes in California, Arizona, New Mexico, and Utah desiccated (McGee et al., 2018). Offshore western North America, the weakening of the Aleutian Low reduced the influx of polar water into the Santa Barbara Basin, causing SSTs there to warm (Hendy and Kennett, 2000; Hendy et al., 2002;

https://doi.org/10.5194/egusphere-2025-1370
Preprint. Discussion started: 3 April 2025

Hendy, 2010), and the northward repositioning of the northeastern Pacific's subtropical high shutdown upwelling in the Gulf of California, allowing subtropical water to enter the Gulf and warm SSTs there (Ganeshram and Pedersen, 1998; McClymont et al., 2012).

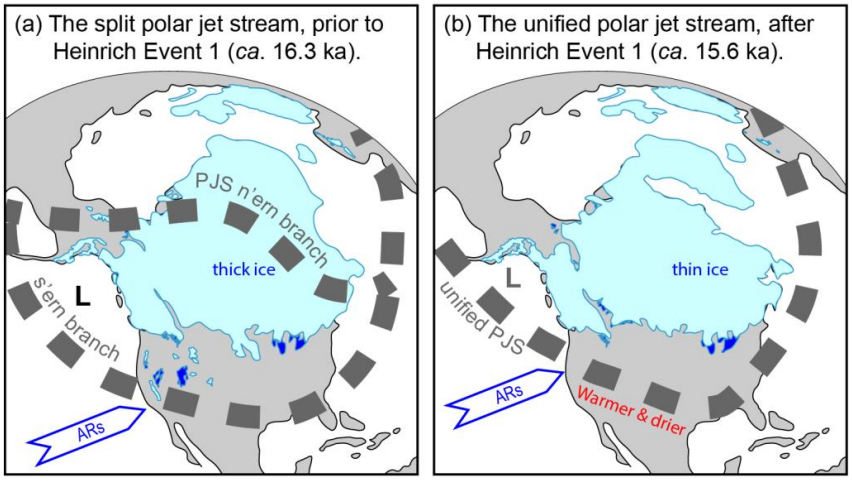

Figure 9. Cartoon illustrating how we propose the polar jet stream evolved in response to Heinrich Event 1 and how we envision the principal location in landfalling atmospheric rivers (ARs) changed. The removal of ice from the Laurentide Ice Sheet and the ice sheet's associated height reduction facilitated reunification of the polar jet stream (PJS) and a northward shift in its mean position (relative to its southern branch's former position). This reorganization in atmospheric circulation brought warmer and drier conditions to California and the southern Great Basin, driving the Tioga 4 deglaciation in the Sierra Nevada and the abandonment of lake-level highstands in the southern Great Basin. Ice sheet and lake reconstructions simplified from Dyke et al. (2003).

https://doi.org/10.5194/egusphere-2025-1370
Preprint. Discussion started: 3 April 2025

6. Conclusions

We present thirty-one new ^{10}Be and twenty-six recalculated ^{36}Cl dates (Phillips et al., 2009) on the timing and duration of the Tioga 4 deglaciation in the Sierra Nevada Mountains of California. We calculate these dates using three different surface-exposure calculators [the Version 3 calculator (Balco et al., 2008), CRONUScalc 2.0 (Marrero et al., 2016), and CREp (Martin et al., 2017)] and we interpret that the CRONUScalc and CREp results (which are essentially identical) are a few percent more accurate (~5 %) than the results from the Version 3 calculator for the samples in this dataset. Adopting the CRONUScalc results as our preferred set of surface-exposure dates, we find that the Tioga 4 deglaciation – which followed the last major Pleistocene readvance in the Sierra Nevada and essentially deglaciated the range – began at 16.4 ± 0.8 ka (n = 7). Furthermore, we find that the range deglaciated in ca. 1.0 kyr (median estimate, with a 95% confidence range of 0.2–3.0 kyr).

In addition, we use Bchron 4.7.6 (Haslett and Parnell, 2008) to construct new age-depth models for the paleoenvironmental record from Swamp Lake (Fig. S23; Table S7; Street et al., 2012) and for speleothem ML1 from McLean's Cave (Fig. S25; Table S9; Oster et al., 2015). The principal benefit of these new age-depth models is that they provide age-uncertainty estimates for the undated horizons in these records, which the original age-depth models lacked. Examining the 16.4 ± 0.8 ka portions of these records, we find evidence of warming at 16.4 ± 0.4 ka in the Swamp Lake core (with no commentary on potential precipitation changes) and evidence of drying (and possibly also warming) at 16.20 ± 0.13 ka in the McLean's Cave speleothem. These three events – the onset of the Tioga 4 deglaciation, as recorded by ^{10}Be and ^{36}Cl concentrations in morainal boulders, the warming recorded at Swamp Lake, and the drying recorded at McLean's Cave – are indistinguishable in age and we interpret them to be different

https://doi.org/10.5194/egusphere-2025-1370
Preprint. Discussion started: 3 April 2025

manifestations of the same event: a warming and drying of the central Sierra Nevada that started at 16.20 ± 0.13 ka.

We place the warming and drying of the central Sierra Nevada (36–38° N) in a regional context by comparing it with the timing of lake-level highstands in the Great Basin (Munroe and Laabs, 2013; Ibarra et al., 2014) and with the start of rising SSTs in the Santa Barbara Basin (Hendy et al., 2002) and the Gulf of California (McClymont et al., 2012). We find evidence indicating a ~6° northward shift in the mean latitude of landfalling atmospheric rivers at ca. 16.2 ka.

Finally, we hypothesize that the Sierra Nevada's deglaciation and the southern Great Basin's desiccation were the result of Heinrich Event 1 (Heinrich, 1988; Hemming, 2004) – which started at 16.22 ± 0.04 ka and ended at 16.04 ± 0.04 ka (Bernal-Wormull et al., 2021; Pérez-Mejías et al., 2021) – reducing the height and extent of the Laurentide Ice Sheet such that it no longer split the polar jet stream into northern and southern branches as it passed over North America. The polar jet stream reunified in response to a thinner and smaller ice sheet, and adopted a more northerly position (as compared with the mean position of the jet stream's former southern branch), bringing warmer and drier weather to California and the southern Great Basin, driving the Tioga 4 deglaciation, lowering lake levels throughout the region, and warming SSTs in the Santa Barbara Basin and the Gulf of California.

https://doi.org/10.5194/egusphere-2025-1370
Preprint. Discussion started: 3 April 2025

Data availability

The data necessary to recalculate the surface-exposure ages of the new ^{10}Be concentrations reported here are available in this article's online supplement. The supplement also contains field photos of the sampled boulders and the new age-depth models we report for the Swamp Lake and McLean's Cave paleoenvironmental reconstructions. The necessary files to reproduce the snow-shielding calculations are available at: https://github.com/BerylliumBecker/SierraNevadaSnowDepths.

Author contributions

RAB conceptualized the study. RAB, SAM, BT, and MWC secured the funding for fieldwork and lab analyses. RAB collected the boulders for ^{10}Be dating, with the aid of field assistants acknowledged below. RAB and AMB processed the samples for ^{10}Be, with the aid of lab assistants acknowledged below. MWC and PRIME Lab colleagues measured ^{10}Be/^{9}Be in the samples. RAB calculated the snow-shielding correction factors, developed the new age-depth models for the Swamp Lake and McLean's Cave paleoenvironmental reconstructions, and recalculated the ages of legacy ^{36}Cl and ^{14}C data. RAB, AMC, SAM, and BT interpreted the results. RAB wrote the manuscript's first draft and created the figures and tables. All the authors edited the manuscript.

Competing interests

The authors declare that they have no competing interests.

https://doi.org/10.5194/egusphere-2025-1370
Preprint. Discussion started: 3 April 2025

Acknowledgements

Sampling permission was granted by the citizens of the United States, via their representatives in the National Park Service and the U.S. Forest Service. We thank Greg Stock (Yosemite National Park) and USFS District Ranger Ray Porter (Sierra National Forest) for their help in navigating the permitting process. JT Holcombe, Will Montz, and Michael Bahrmasel helped collect the ^{10}Be samples. Alexander Horvath, Levi Mitchell, and Elizabeth Ceperley assisted with the laboratory work. We thank them all. Funding was provided by the UW-Madison Department of Geoscience, AAPG Foundation's Robert and Carolyn Maby Memorial Grant, a Geological Society of America student research grant, and a Doctoral Dissertation Improvement Award from the National Science Foundation (grant #1303194).

https://doi.org/10.5194/egusphere-2025-1370
Preprint. Discussion started: 3 April 2025

7. *References*

Ackert, R. P., Becker, R. A., Singer, B. S., Kurz, M. D., Caffee, M. W., and Mickelson, D. M.: Patagonian glacier response during the Late Glacial–Holocene transition, Science, 321, 392–395, 2008.

Allen, B. D. and Anderson, R. Y.: A continuous, high-resolution record of late Pleistocene climate variability from the Estancia basin, New Mexico, Geological Society of America Bulletin, 112, 1444–1458, 2000.

Alley, R. B.: The Younger Dryas cold interval as viewed from central Greenland, Quaternary Science Reviews, 19, 213–226, 2000.

Amos, C. B., Kelson, K. I., Rood, D. H., Simpson, D. T., and Rose, R. S.: Late Quaternary slip rate on the Kern Canyon fault at Soda Spring, Tulare County, California, Lithosphere, 2, 411–417, 2010.

Bahr, A., Hoffmann, J., Schönfeld, J., Schmidt, M. W., Nürnberg, D., Batenburg, S. J., and Voigt, S.: Low-latitude expressions of high-latitude forcing during Heinrich Stadial 1 and the Younger Dryas in northern South America, Global and Planetary Change, 160, 1–9, 2018.

Balco, G.: Contributions and unrealized potential contributions of cosmogenic-nuclide exposure dating to glacier chronology, 1990–2010, Quaternary Science Reviews, 30, 3–27, 2011.

Balco, G.: Elevation/atmospheric pressure models, The bleeding edge of cosmogenic-nuclide geochemistry, https://cosmognosis.wordpress.com/2015/10/16/elevationatmospheric-pressure-models/, 2015.

Balco, G.: Saturated surfaces in Antarctica, The bleeding edge of cosmogenic-nuclide geochemistry, https://cosmognosis.wordpress.com/2016/09/09/saturated-surfaces-in-antarctica/, 2016.

Balco, G.: Where's the reference production rate?, The bleeding edge of cosmogenic-nuclide geochemistry, https://cosmognosis.wordpress.com/2018/09/06/wheres-the-reference-production-rate/, 2018.

Balco, G., Stone, J. O., Lifton, N. A., and Dunai, T. J.: A complete and easily accessible means of calculating surface exposure ages or erosion rates from ^{10}Be and ^{26}Al measurements, Quaternary Geochronology, 3, 174–195, 2008.

Barth, A. M., Clark, P. U., Clark, J., Roe, G. H., Marcott, S. A., McCabe, A. M., Caffee, M. W., He, F., Cuzzone, J. K., and Dunlop, P.: Persistent millennial-scale glacier fluctuations in Ireland between 24 ka and 10 ka, Geology, 46, 151–154, 2018.

Barth, A. M., Marcott, S. A., Licciardi, J. M., and Shakun, J. D.: Deglacial Thinning of the Laurentide Ice Sheet in the Adirondack Mountains, New York, USA, Revealed by ^{36}Cl Exposure Dating, Paleoceanography and Paleoclimatology, 34, 946–953, https://doi.org/10.1029/2018PA003477, 2019.

https://doi.org/10.5194/egusphere-2025-1370
Preprint. Discussion started: 3 April 2025

Bartlein, P. J., Anderson, K. H., Anderson, P. M., Edwards, M. E., Mock, C. J., Thompson, R. S., Webb, R. S., Webb III, T., and Whitlock, C.: Paleoclimate simulations for North America over the past 21,000 years: features of the simulated climate and comparisons with paleoenvironmental data, Quaternary science reviews, 17, 549–585, 1998.

Bateman, P. C. and Wones, D. R.: Geologic map of the Huntington Lake quadrangle, central Sierra Nevada, California, 1972.

Bateman, P. C., Kistler, Ronald W., Peck, Dallas L., and Busacca, Alan: Geologic map of the Tuolumne Meadows quadrangle, Yosemite National Park, California, 1983.

Benson, L. V., Burdett, J. W., Kashgarian, M., Lund, S. P., Phillips, F. M., and Rye, R. O.: Climatic and Hydrologic Oscillations in the Owens Lake Basin and Adjacent Sierra Nevada, California, Science, 274, 746–749, https://doi.org/10.1126/science.274.5288.746, 1996.

Bernal-Wormull, J. L., Moreno, A., Pérez-Mejías, C., Bartolomé, M., Aranburu, A., Arriolabengoa, M., Iriarte, E., Cacho, I., Spötl, C., and Edwards, R. L.: Immediate temperature response in northern Iberia to last deglacial changes in the North Atlantic, Geology, 49, 999–1003, 2021.

Bierman, P. R., Davis, P. T., Corbett, L. B., Lifton, N. A., and Finkel, R. C.: Cold-based Laurentide ice covered New England's highest summits during the Last Glacial Maximum, Geology, 43, 1059–1062, https://doi.org/10.1130/G37225.1, 2015.

Birman, J. H.: Glacial geology across the crest of the Sierra Nevada, California, Geological Society of America Special Paper, 75, 1964.

Blackwelder, E.: Pleistocene glaciation in the Sierra Nevada and Basin ranges, Bulletin of the Geological Society of America, 42, 865–922, 1931.

Borchers, B., Marrero, S., Balco, G., Caffee, M., Goehring, B., Lifton, N., Nishiizumi, K., Phillips, F., Schaefer, J., and Stone, J.: Geological calibration of spallation production rates in the CRONUS-Earth project, Quaternary Geochronology, 31, 188–198, 2016.

Bromwich, D. H., Toracinta, E. R., Wei, H., Oglesby, R. J., Fastook, J. L., and Hughes, T. J.: Polar MM5 simulations of the winter climate of the Laurentide Ice Sheet at the LGM, Journal of Climate, 17, 3415–3433, 2004.

Chiang, J. C., Lee, S.-Y., Putnam, A. E., and Wang, X.: South Pacific Split Jet, ITCZ shifts, and atmospheric North–South linkages during abrupt climate changes of the last glacial period, Earth and Planetary Science Letters, 406, 233–246, 2014.

Clark, D., Gillespie, A. R., Clark, M., and Burke, B.: Mountain glaciations of the Sierra Nevada, in: Quaternary Geology of the United States, Desert Research Institute, Reno, NV, 287–311, 2003.

https://doi.org/10.5194/egusphere-2025-1370
Preprint. Discussion started: 3 April 2025

Clark, D. H. and Clark, M. M.: New evidence of late-Wisconsin deglaciation in the Sierra Nevada, California, refutes the Hilgard Glaciation, in: Geological Society of America, Abstracts with Programs, 1995.

Clark, D. H. and Gillespie, A. R.: Timing and significance of Late-Glacial and Holocene cirque glaciation in the Sierra Nevada, California, Quaternary International, 38, 21–38, 1997.

Clark, D. H., Bierman, P. R., and Larsen, P.: Improving in situ cosmogenic chronometers, Quaternary Research, 44, 367–377, 1995.

Clark, M.: Evidence for rapid destruction of Latest Pleistocene glaciers of the Sierra Nevada, California, in: Geological Society of America, Abstracts with Programs, 361–362, 1976.

Clark, P. U., Shakun, J. D., Baker, P. A., Bartlein, P. J., Brewer, S., Brook, E., Carlson, A. E., Cheng, H., Kaufman, D. S., Liu, Z., Marchitto, T. M., Mix, A. C., Morrill, C., Otto-Bliesner, B. L., Pahnke, K., Russell, J. M., Whitlock, C., Adkins, J. F., Blois, J. L., Clark, J., Colman, S. M., Curry, W. B., Flower, B. P., He, F., Johnson, T. C., Lynch-Stieglitz, J., Markgraf, V., McManus, J., Mitrovica, J. X., Moreno, P. I., and Williams, J. W.: Global climate evolution during the last deglaciation, Proceedings of the National Academy of Sciences, 109, https://doi.org/10.1073/pnas.1116619109, 2012.

Corbett, L. B., Bierman, P. R., Wright, S. F., Shakun, J. D., Davis, P. T., Goehring, B. M., Halsted, C. T., Koester, A. J., Caffee, M. W., and Zimmerman, S. R.: Analysis of multiple cosmogenic nuclides constrains Laurentide Ice Sheet history and process on Mt. Mansfield, Vermont's highest peak, Quaternary Science Reviews, 205, 234–246, https://doi.org/10.1016/j.quascirev.2018.12.014, 2019.

Cushing, H. P.: Notes on the Muir Glacier region, and its geology, The American Geologist, 8, 207–230, 1891.

Dansgaard, W., Johnsen, S. J., Clausen, H. B., Dahl-Jensen, D., Gundestrup, N. S., Hammer, C. U., Hvidberg, C. S., Steffensen, J. P., Sveinbjörnsdottir, A. E., and Jouzel, J.: Evidence for general instability of past climate from a 250-kyr ice-core record, Nature, 364, 218–220, 1993.

Davis, P. T., Bierman, P. R., Corbett, L. B., and Finkel, R. C.: Cosmogenic exposure age evidence for rapid Laurentide deglaciation of the Katahdin area, west-central Maine, USA, 16 to 15 ka, Quaternary Science Reviews, 116, 95–105, https://doi.org/10.1016/j.quascirev.2015.03.021, 2015.

Davis, P. T., Halsted, C. T., Rogers, J. N., Arcone, S. A., Shakun, J. D., Bierman, P. R., Corbett, L. B., and Koester, A. J.: Glacial, deglacial, and postglacial history of Franconia Notch, NH, from constructing a cosmogenic nuclide glacial dipstick to determining a landslide history from lake sediment cores and ground penetrating radar images, in: Guidebook for field trips in central Vermont and adjoining New Hampshire, vol. 111th Annual Meeting, 235–286, 2019.

Deevey, E. S., Gross, M. S., Hutchinson, G. E., and Kraybill, H. L.: The natural C-14 contents of materials from hard-water lakes, Proceedings of the National Academy of Sciences, 40, 285–288, 1954.

https://doi.org/10.5194/egusphere-2025-1370
Preprint. Discussion started: 3 April 2025

Denton, G. H. and Karlén, W.: Holocene Glacial and tree-line variations in the White River Valley and Skolai Pass, Alaska and Yukon Territory, Quaternary Research, 7, 63–111, 1977.

Denton, G. H., Anderson, R. F., Toggweiler, J. R., Edwards, R. L., Schaefer, J. M., and Putnam, A. E.: The Last Glacial Termination, Science, 328, 1652–1656, https://doi.org/10.1126/science.1184119, 2010.

Douglass, D. C., Singer, B. S., Kaplan, M. R., Mickelson, D. M., and Caffee, M. W.: Cosmogenic nuclide surface exposure dating of boulders on last-glacial and late-glacial moraines, Lago Buenos Aires, Argentina: Interpretive strategies and paleoclimate implications, Quaternary Geochronology, 1, 43–58, 2006.

Drebber, J. S., Halsted, C. T., Corbett, L. B., Bierman, P. R., and Caffee, M. W.: In Situ Cosmogenic ^{10}Be Dating of Laurentide Ice Sheet Retreat from Central New England, USA, Geosciences, 13, 213, https://doi.org/10.3390/geosciences13070213, 2023.

Dühnforth, M., Anderson, R. S., Ward, D., and Stock, G. M.: Bedrock fracture control of glacial erosion processes and rates, Geology, 38, 423–426, 2010.

Dyke, A. S., Moore, A., and Robertson, L.: Deglaciation of North America, Geological Survey of Canada Open File Report, 1574, https://doi.org/10.4095/214399, 2003.

Farber, D. L., Hancock, G. S., Finkel, R. C., and Rodbell, D. T.: The age and extent of tropical alpine glaciation in the Cordillera Blanca, Peru, Journal of Quaternary Science, 20, 759–776, https://doi.org/10.1002/jqs.994, 2005.

Field, W. O. Jr.: Glacier recession in Muir Inlet, Glacier Bay, Alaska, Geographical Review, 37, 349–399, 1947.

Firestone, R. B., West, A., Kennett, J. P., Becker, L., Bunch, T. E., Revay, Z. S., Schultz, P. H., Belgya, T., Kennett, D. J., Erlandson, J. M., Dickenson, O. J., Goodyear, A. C., Harris, R. S., Howard, G. A., Kloosterman, J. B., Lechler, P., Mayewski, P. A., Montgomery, J., Poreda, R., Darrah, T., Hee, S. S. Q., Smith, A. R., Stich, A., Topping, W., Wittke, J. H., and Wolbach, W. S.: Evidence for an extraterrestrial impact 12,900 years ago that contributed to the megafaunal extinctions and the Younger Dryas cooling, Proceedings of the National Academy of Sciences, 104, 16016–16021, https://doi.org/10.1073/pnas.0706977104, 2007.

Ganeshram, R. S. and Pedersen, T. F.: Glacial-interglacial variability in upwelling and bioproductivity off NW Mexico: Implications for Quaternary paleoclimate, Paleoceanography, 13, 634–645, 1998.

Ganopolski, A. and Rahmstorf, S.: Rapid changes of glacial climate simulated in a coupled climate model, Nature, 409, 153–158, 2001.

Godwin, H.: Comments on radiocarbon dating for samples from the British Isles, American Journal of Science, 249, 301–307, 1951.

https://doi.org/10.5194/egusphere-2025-1370
Preprint. Discussion started: 3 April 2025

Goldthwait, J. W.: The uncovering of New Hampshire by the last ice sheet, American Journal of Science, 236, 345–372, 1938.

Goldthwait, R. P. and Mickelson, D. M.: Glacier Bay, a model for the deglaciation of the White Mountains in New Hampshire, Ohio State University, Institute of Polar Studies, 1982.

Gosse, J. C. and Phillips, F. M.: Terrestrial in situ cosmogenic nuclides: theory and application, Quaternary Science Reviews, 20, 1475–1560, 2001.

Gosse, J. C., Evenson, E. B., Klein, J., Lawn, B., and Middleton, R.: Precise cosmogenic ^{10}Be measurements in western North America: Support for a global Younger Dryas cooling event, Geology, 23, 877–880, 1995.

Halsted, C. T., Bierman, P. R., Shakun, J. D., Davis, P. T., Corbett, L. B., Drebber, J. S., and Ridge, J. C.: A critical re-analysis of constraints on the timing and rate of Laurentide Ice Sheet recession in the northeastern United States, Journal of Quaternary Science, 39, 54–69, https://doi.org/10.1002/jqs.3563, 2024.

Haslett, J. and Parnell, A.: A simple monotone process with application to radiocarbon-dated depth chronologies, Journal of the Royal Statistical Society Series C: Applied Statistics, 57, 399–418, 2008.

He, F., Shakun, J. D., Clark, P. U., Carlson, A. E., Liu, Z., Otto-Bliesner, B. L., and Kutzbach, J. E.: Northern Hemisphere forcing of Southern Hemisphere climate during the last deglaciation, Nature, 494, 81–85, 2013.

Heinrich, H.: Origin and consequences of cyclic ice rafting in the northeast Atlantic Ocean during the past 130,000 years, Quaternary Research, 29, 142–152, 1988.

Hemming, S. R.: Heinrich events: Massive Late Pleistocene detritus layers of the North Atlantic and their global climate imprint, Reviews of Geophysics, 42, 2003RG000128, https://doi.org/10.1029/2003RG000128, 2004.

Hendy, I. L.: The paleoclimatic response of the Southern California Margin to the rapid climate change of the last 60 ka: A regional overview, Quaternary International, 215, 62–73, 2010.

Hendy, I. L. and Kennett, J. P.: Dansgaard-Oeschger cycles and the California Current System: planktonic foraminiferal response to rapid climate change in Santa Barbara Basin, Ocean Drilling Program hole 893A, Paleoceanography, 15, 30–42, 2000.

Hendy, I. L., Kennett, J. P., Roark, E. B., and Ingram, B. L.: Apparent synchroneity of submillennial scale climate events between Greenland and Santa Barbara Basin, California from 30–10 ka, Quaternary Science Reviews, 21, 1167–1184, 2002.

Huber, N. K.: Preliminary geologic map of the Dardanelles Cone quadrangle, central Sierra Nevada, California, 1983.

Huber, N. K.: Geological Ramblings in Yosemite, Yosemite Conservancy, 136 pp., 2007.

https://doi.org/10.5194/egusphere-2025-1370
Preprint. Discussion started: 3 April 2025

Ibarra, D. E., Egger, A. E., Weaver, K. L., Harris, C. R., and Maher, K.: Rise and fall of late Pleistocene pluvial lakes in response to reduced evaporation and precipitation: Evidence from Lake Surprise, California, Geological Society of America Bulletin, 126, 1387–1415, 2014.

James, L. A., Harbor, J., Fabel, D., Dahms, D., and Elmore, D.: Late Pleistocene glaciations in the northwestern Sierra Nevada, California, Quaternary Research, 57, 409–419, 2002.

Jones, T. R., Roberts, W. H., Steig, E. J., Cuffey, K. M., Markle, B. R., and White, J. W. C.: Southern Hemisphere climate variability forced by Northern Hemisphere ice-sheet topography, Nature, 554, 351–355, 2018.

Jouzel, J., Vaikmae, R., Petit, J. R., Martin, M., Duclos, Y., Stievenard, M., Lorius, C., Toots, M., Mélières, M. A., Burckle, L. H., Barkov, N. I., and Kotlyakov, V. M.: The two-step shape and timing of the last deglaciation in Antarctica, Climate Dynamics, 11, 151–161, https://doi.org/10.1007/BF00223498, 1995.

Kelly, M. A., Lowell, T. V., Applegate, P. J., Phillips, F. M., Schaefer, J. M., Smith, C. A., Kim, H., Leonard, K. C., and Hudson, A. M.: A locally calibrated, late glacial ^{10}Be production rate from a low-latitude, high-altitude site in the Peruvian Andes, Quaternary Geochronology, 26, 70–85, 2015.

Koester, A. J., Shakun, J. D., Bierman, P. R., Davis, P. T., Corbett, L. B., Braun, D., and Zimmerman, S. R.: Rapid thinning of the Laurentide Ice Sheet in coastal Maine, USA, during late Heinrich Stadial 1, Quaternary Science Reviews, 163, 180–192, https://doi.org/10.1016/j.quascirev.2017.03.005, 2017.

Koester, A. J., Shakun, J. D., Bierman, P. R., Davis, P. T., Corbett, L. B., Goehring, B. M., Vickers, A. C., and Zimmerman, S. R.: Laurentide Ice Sheet thinning and erosive regimes at Mount Washington, New Hampshire, inferred from multiple cosmogenic nuclides, in: Untangling the Quaternary Period—A Legacy of Stephen C. Porter, vol. 548, edited by: Waitt, R. B., Thackray, G. D., and Gillespie, A. R., Geological Society of America, https://doi.org/10.1130/2020.2548(15), 2021.

Kullman, L.: Late Holocene reproductional patterns of *Pinus sylvestris* and *Picea abies* at the forest limit in central Sweden, Canadian Journal of Botany, 64, 1682–1690, https://doi.org/10.1139/b86-225, 1986.

Kullman, L.: New and firm evidence for Mid-Holocene appearance of *Picea abies* in the Scandes Mountains, Sweden, Journal of Ecology, 439–447, 1995.

Kutzbach, J. E. and Guetter, P. J.: The influence of changing orbital parameters and surface boundary conditions on climate simulations for the past 18 000 years, Journal of atmospheric sciences, 43, 1726–1759, 1986.

Kutzbach, J. E. and Wright Jr, H. E.: Simulation of the climate of 18,000 years BP: Results for the North American/North Atlantic/European sector and comparison with the geologic record of North America, Quaternary Science Reviews, 4, 147–187, 1985.

https://doi.org/10.5194/egusphere-2025-1370
Preprint. Discussion started: 3 April 2025

Laabs, B. J., Marchetti, D. W., Munroe, J. S., Refsnider, K. A., Gosse, J. C., Lips, E. W., Becker, R. A., Mickelson, D. M., and Singer, B. S.: Chronology of latest Pleistocene mountain glaciation in the western Wasatch Mountains, Utah, USA, Quaternary Research, 76, 272–284, 2011.

Laabs, B. J., Licciardi, J. M., Leonard, E. M., Munroe, J. S., and Marchetti, D. W.: Updated cosmogenic chronologies of Pleistocene mountain glaciation in the western United States and associated paleoclimate inferences, Quaternary Science Reviews, 242, 106427, 2020.

Lal, D.: Cosmic ray labeling of erosion surfaces: in situ nuclide production rates and erosion models, Earth and Planetary Science Letters, 104, 424–439, 1991.

LaMarche, V. C. and Mooney, H. A.: Altithermal timberline advance in western United States, Nature, 213, 980–982, 1967.

Lemieux-Dudon, B., Blayo, E., Petit, J.-R., Waelbroeck, C., Svensson, A., Ritz, C., Barnola, J.-M., Narcisi, B. M., and Parrenin, F.: Consistent dating for Antarctic and Greenland ice cores, Quaternary Science Reviews, 29, 8–20, 2010.

Leonard, E. M., Laabs, B. J., Marcott, S. A., Crawford, E. E., Mackall, B. T., Ibarra, D. E., Osman, M. B., Plummer, M. A., and Caffee, M. W.: Chronology and climate of the Last Glacial Maximum and the subsequent deglaciation in the northern Medicine Bow Mountains, Wyoming, USA, Quaternary Science Advances, 12, 100109, 2023.

Li, C. and Born, A.: Coupled atmosphere-ice-ocean dynamics in Dansgaard-Oeschger events, Quaternary Science Reviews, 203, 1–20, 2019.

Lifton, N.: Implications of two Holocene time-dependent geomagnetic models for cosmogenic nuclide production rate scaling, Earth and Planetary Science Letters, 433, 257–268, 2016.

Lifton, N., Sato, T., and Dunai, T. J.: Scaling in situ cosmogenic nuclide production rates using analytical approximations to atmospheric cosmic-ray fluxes, Earth and Planetary Science Letters, 386, 149–160, 2014.

Lifton, N., Caffee, M., Finkel, R., Marrero, S., Nishiizumi, K., Phillips, F. M., Goehring, B., Gosse, J., Stone, J., and Schaefer, J.: In situ cosmogenic nuclide production rate calibration for the CRONUS-Earth project from Lake Bonneville, Utah, shoreline features, Quaternary Geochronology, 26, 56–69, 2015.

Löfverström, M., Caballero, R., Nilsson, J., and Kleman, J.: Evolution of the large-scale atmospheric circulation in response to changing ice sheets over the last glacial cycle, Climate of the Past, 10, 1453–1471, 2014.

Lora, J. M., Mitchell, J. L., and Tripati, A. E.: Abrupt reorganization of North Pacific and western North American climate during the last deglaciation, Geophysical Research Letters, 43, 11–796, 2016.

Lowell, T. V.: Late Wisconsin ice-flow reversal and deglaciation, northwestern Maine, Geological Society of America Special Paper, 197, 71–83, 1985.

https://doi.org/10.5194/egusphere-2025-1370
Preprint. Discussion started: 3 April 2025

Lowell, T. V., Kite, J. S., Calkin, P. E., and Halter, E. F.: Analysis of small-scale erosional data and a sequence of late Pleistocene flow reversal, northern New England, Geological Society of America Bulletin, 102, 74–85, 1990.

Manabe, S. and Broccoli, A. J.: The influence of continental ice sheets on the climate of an ice age, Journal of Geophysical Research: Atmospheres, 90, 2167–2190, https://doi.org/10.1029/JD090iD01p02167, 1985.

Mangerud, J.: The discovery of the Younger Dryas, and comments on the current meaning and usage of the term, Boreas, 50, 1–5, https://doi.org/10.1111/bor.12481, 2021.

Mangerud, J., Andersen, S. T., Berglund, B. E., and Donner, J. J.: Quaternary stratigraphy of Norden, a proposal for terminology and classification, Boreas, 3, 109–126, https://doi.org/10.1111/j.1502-3885.1974.tb00669.x, 1974.

Marcott, S. A., Shakun, J. D., Clark, P. U., and Mix, A. C.: A reconstruction of regional and global temperature for the past 11,300 Years, Science, 339, 1198–1201, https://doi.org/10.1126/science.1228026, 2013.

Marcott, S. A., Clark, P. U., Shakun, J. D., Brook, E. J., Davis, P. T., and Caffee, M. W.: 10Be age constraints on latest Pleistocene and Holocene cirque glaciation across the western United States, npj Climate and Atmospheric Science, 5, 1–7, 2019.

Marrero, S.: Calibration of cosmogenic chlorine-36, PhD Thesis, New Mexico Institute of Mining and Technology, Socorro, NM, 365 pp., 2012.

Marrero, S. M., Phillips, F. M., Borchers, B., Lifton, N., Aumer, R., and Balco, G.: Cosmogenic nuclide systematics and the CRONUScalc program, Quaternary Geochronology, 31, 160–187, 2016.

Martin, L. C. P., Blard, P.-H., Balco, G., Lavé, J., Delunel, R., Lifton, N., and Laurent, V.: The CREp program and the ICE-D production rate calibration database: A fully parameterizable and updated online tool to compute cosmic-ray exposure ages, Quaternary Geochronology, 38, 25–49, 2017.

Mayewski, P. A., Rohling, E. E., Stager, J. C., Karlén, W., Maasch, K. A., Meeker, L. D., Meyerson, E. A., Gasse, F., van Kreveld, S., and Holmgren, K.: Holocene climate variability, Quaternary Research, 62, 243–255, 2004.

McClymont, E. L., Ganeshram, R. S., Pichevin, L. E., Talbot, H. M., Van Dongen, B. E., Thunell, R. C., Haywood, A. M., Singarayer, J. S., and Valdes, P. J.: Sea-surface temperature records of Termination 1 in the Gulf of California: Challenges for seasonal and interannual analogues of tropical Pacific climate change, Paleoceanography, 27, 2011PA002226, https://doi.org/10.1029/2011PA002226, 2012.

McGee, D., Moreno-Chamarro, E., Marshall, J., and Galbraith, E. D.: Western U.S. lake expansions during Heinrich stadials linked to Pacific Hadley circulation, Science Advances, 4, eaav0118, https://doi.org/10.1126/sciadv.aav0118, 2018.

https://doi.org/10.5194/egusphere-2025-1370
Preprint. Discussion started: 3 April 2025

Mickelson, D. M.: Glacial geology of the Burroughs Glacier area, southeastern Alaska, Ph.D. Dissertation, The Ohio State University, Columbus, OH, 240 pp., 1971.

Moore, J. G.: Geologic map of the Mount Whitney quadrangle, Inyo and Tulare counties, California, United States Geological Survey, 1981.

Munroe, J. S. and Laabs, B. J.: Temporal correspondence between pluvial lake highstands in the southwestern US and Heinrich Event 1, Journal of Quaternary Science, 28, 49–58, 2013.

Nishiizumi, K., Winterer, E. L., Kohl, C. P., Klein, J., Middleton, R., Lal, D., and Arnold, J. R.: Cosmic ray production rates of ^{10}Be and ^{26}Al in quartz from glacially polished rocks, Journal of Geophysical Research: Solid Earth, 94, 17907–17915, https://doi.org/10.1029/JB094iB12p17907, 1989.

NOAA, NASA, and USAF: US Standard Atmosphere, 1976, National Oceanic and Atmospheric Administration, 1976.

Oana, S. and Deevey, E. S.: Carbon 13 in lake waters, and its possible bearing on paleolimnology, American Journal of Science, 258-A, 253–272, 1960.

Oerlemans, J.: Extracting a climate signal from 169 glacier records, Science, 308, 675–677, 2005.

Oster, J. L., Montanez, I. P., Santare, L. R., Sharp, W. D., Wong, C., and Cooper, K. M.: Stalagmite records of hydroclimate in central California during termination 1, Quaternary Science Reviews, 127, 199–214, 2015.

Otto-Bliesner, B. L., Brady, E. C., Clauzet, G., Tomas, R., Levis, S., and Kothavala, Z.: Last glacial maximum and Holocene climate in CCSM3, Journal of Climate, 19, 2526–2544, 2006.

Pedro, J. B., Jochum, M., Buizert, C., He, F., Barker, S., and Rasmussen, S. O.: Beyond the bipolar seesaw: Toward a process understanding of interhemispheric coupling, Quaternary Science Reviews, 192, 27–46, 2018.

Peltier, W. R.: Global glacial isostasy and the surface of the Ice-Age Earth: The ICE-5G (VM2) model and GRACE, Annual Review of Earth and Planetary Sciences, 32, 111–149, https://doi.org/10.1146/annurev.earth.32.082503.144359, 2004.

Pérez-Mejías, C., Moreno, A., Bernal-Wormull, J., Cacho, I., Osácar, M. C., Edwards, R. L., and Cheng, H.: Oldest Dryas hydroclimate reorganization in the eastern Iberian Peninsula after the iceberg discharges of Heinrich Event 1, Quaternary Research, 101, 67–83, 2021.

Peteet, D., Del Genio, A., and Lo, K. K. -W.: Sensitivity of Northern Hemisphere air temperatures and snow expansion to North Pacific sea surface temperatures in the Goddard Institute for Space Studies general circulation model, Journal of Geophysical Research: Atmospheres, 102, 23781–23791, https://doi.org/10.1029/97JD01573, 1997.

https://doi.org/10.5194/egusphere-2025-1370
Preprint. Discussion started: 3 April 2025

Philippsen, B.: The freshwater reservoir effect in radiocarbon dating, Heritage Science, 1, 1–19, 2013.

Phillips, F. M.: Cosmogenic nuclide data sets from the Sierra Nevada, California, for assessment of nuclide production models: I. Late Pleistocene glacial chronology, Quaternary Geochronology, 35, 119–129, 2016.

Phillips, F. M., Zreda, M. G., Benson, L. V., Plummer, M. A., Elmore, D., and Sharma, P.: Chronology for fluctuations in Late Pleistocene Sierra Nevada glaciers and lakes, Science, 274, 749–751, 1996.

Phillips, F. M., Stone, W. D., and Fabryka-Martin, J. T.: An improved approach to calculating low-energy cosmic-ray neutron fluxes near the land/atmosphere interface, Chemical Geology, 175, 689–701, 2001.

Phillips, F. M., Zreda, M., Plummer, M. A., Elmore, D., and Clark, D. H.: Glacial geology and chronology of Bishop Creek and vicinity, eastern Sierra Nevada, California, Geological Society of America Bulletin, 121, 1013–1033, 2009.

Phillips, F. M., Kelly, M. A., Hudson, A. M., Stone, J. O., Schaefer, J., Marrero, S. M., Fifield, L. K., Finkel, R., and Lowell, T.: CRONUS-Earth calibration samples from the Huancané II moraines, Quelccaya ice cap, Peru, Quaternary Geochronology, 31, 220–236, 2016.

Power, M. J.: Paleoclimatic interpretation of an alpine lake in south central Sierra Nevada, California, multiple proxy evidence, MS thesis, Northern Arizona University, 1998.

Praetorius, S. K., Condron, A., Mix, A. C., Walczak, M. H., McKay, J. L., and Du, J.: The role of Northeast Pacific meltwater events in deglacial climate change, Science Advances, 6, eaay2915, https://doi.org/10.1126/sciadv.aay2915, 2020.

Putnam, A. E., Denton, G. H., Schaefer, J. M., Barrell, D. J., Andersen, B. G., Finkel, R. C., Schwartz, R., Doughty, A. M., Kaplan, M. R., and Schlüchter, C.: Glacier advance in southern middle-latitudes during the Antarctic Cold Reversal, Nature Geoscience, 3, 700–704, 2010a.

Putnam, A. E., Schaefer, J. M., Barrell, D. J. A., Vandergoes, M., Denton, G. H., Kaplan, M. R., Finkel, R. C., Schwartz, R., Goehring, B. M., and Kelley, S. E.: In situ cosmogenic ^{10}Be production-rate calibration from the Southern Alps, New Zealand, Quaternary Geochronology, 5, 392–409, 2010b.

Quirk, B. J., Moore, J. R., Laabs, B. J., Caffee, M. W., and Plummer, M. A.: Termination II, Last Glacial Maximum, and Lateglacial chronologies and paleoclimate from Big Cottonwood Canyon, Wasatch Mountains, Utah, GSA Bulletin, 130, 1889–1902, 2018.

R Core Team: R: A language and environment for statistical computing, 2024.

Rasmussen, S. O., Bigler, M., Blockley, S. P., Blunier, T., Buchardt, S. L., Clausen, H. B., Cvijanovic, I., Dahl-Jensen, D., Johnsen, S. J., and Fischer, H.: A stratigraphic framework for abrupt climatic changes during the Last Glacial period based on three synchronized Greenland

https://doi.org/10.5194/egusphere-2025-1370
Preprint. Discussion started: 3 April 2025

ice-core records: refining and extending the INTIMATE event stratigraphy, Quaternary Science Reviews, 106, 14–28, 2014.

Reid, H. F.: Glacier Bay and its glaciers, USGS, 1896.

Reimer, P. J., Baillie, M. G., Bard, E., Bayliss, A., Beck, J. W., Bertrand, C. J., Blackwell, P. G., Buck, C. E., Burr, G. S., Cutler, K. B., Damon, P. E., Edwards, R. L., Fairbanks, R. G., Friedrich, M., Guilderson, T. P., Hogg, A. G., Hughen, K. A., Kromer, B., McCormac, G., Manning, S., Ramsey, C. B., Reimer, R. W., Remmele, S., Southon, J. R., Stuiver, M., Talamo, S., Taylor, F. W., Van Der Plicht, J., and Weyhenmeyer, C. E.: IntCal04 terresterial radiocarbon age calibration, 0-26 cal kyr BP, Radiocarbon, 46, 1029–1058, 2004.

Reimer, P. J., Baillie, M. G., Bard, E., Bayliss, A., Beck, J. W., Blackwell, P. G., Ramsey, C. B., Buck, C. E., Burr, G. S., and Edwards, R. L.: IntCal09 and Marine09 radiocarbon age calibration curves, 0–50,000 years cal BP, Radiocarbon, 51, 1111–1150, 2009.

Reimer, P. J., Bard, E., Bayliss, A., Beck, J. W., Blackwell, P. G., Ramsey, C. B., Buck, C. E., Cheng, H., Edwards, R. L., and Friedrich, M.: IntCal13 and Marine13 radiocarbon age calibration curves 0–50,000 years cal BP, Radiocarbon, 55, 1869–1887, 2013.

Reimer, P. J., Austin, W. E., Bard, E., Bayliss, A., Blackwell, P. G., Ramsey, C. B., Butzin, M., Cheng, H., Edwards, R. L., and Friedrich, M.: The IntCal20 Northern Hemisphere radiocarbon age calibration curve (0–55 cal kBP), Radiocarbon, 62, 725–757, 2020.

Rood, D. H., Burbank, D. W., and Finkel, R. C.: Chronology of glaciations in the Sierra Nevada, California, from ^{10}Be surface exposure dating, Quaternary Science Reviews, 30, 646–661, 2011.

Rozanski, K., Araguás-Araguás, L., and Gonfiantini, R.: Isotopic patterns in modern global precipitation, in: Climate Change in Continental Isotopic Records, vol. 78, American Geophysical Union Washington, DC, 1–36, 1993.

Schaefer, J. M., Denton, G. H., Barrell, D. J. A., Ivy-Ochs, S., Kubik, P. W., Andersen, B. G., Phillips, F. M., Lowell, T. V., and Schlüchter, C.: Near-synchronous interhemispheric termination of the Last Glacial Maximum in mid-latitudes, Science, 312, 1510–1513, https://doi.org/10.1126/science.1122872, 2006.

Scuderi, L. A.: Late-Holocene upper timberline variation in the southern Sierra Nevada, Nature, 325, 242–244, 1987.

Shakun, J. D., Clark, P. U., He, F., Marcott, S. A., Mix, A. C., Liu, Z., Otto-Bliesner, B., Schmittner, A., and Bard, E.: Global warming preceded by increasing carbon dioxide concentrations during the last deglaciation, Nature, 484, 49–54, 2012.

Stock, G. M. and Uhrhammer, R. A.: Catastrophic rock avalanche 3600 years BP from El Capitan, Yosemite Valley, California, Earth Surface Processes and Landforms, 35, 941–951, https://doi.org/10.1002/esp.1982, 2010.

https://doi.org/10.5194/egusphere-2025-1370
Preprint. Discussion started: 3 April 2025

1515 Stone, J. O.: Air pressure and cosmogenic isotope production, Journal of Geophysical Research:
1516 Solid Earth, 105, 23753–23759, https://doi.org/10.1029/2000JB900181, 2000.

1517 Street, J. H., Anderson, R. S., and Paytan, A.: An organic geochemical record of Sierra Nevada
1518 climate since the LGM from Swamp Lake, Yosemite, Quaternary Science Reviews, 40, 89–106,
1519 2012.

1520 Stuiver, M. and Reimer, P. J.: Extended ^{14}C data base and revised CALIB 3.0 ^{14}C age calibration
1521 program, Radiocarbon, 35, 215–230, 1993.

1522 Syverson, K. M.: The ability of ice-flow indicators to record complex, historic deglaciation
1523 events, Burroughs Glacier, Alaska, Boreas, 24, 232–244, 1995.

1524 Tulenko, J. P., Briner, J. P., Young, N. E., and Schaefer, J. M.: The last deglaciation of Alaska
1525 and a new benchmark ^{10}Be moraine chronology from the western Alaska Range, Quaternary
1526 Science Reviews, 287, 107549, 2022.

1527 Uppala, S. M., Kållberg, P. W., Simmons, A. J., Andrae, U., Bechtold, V. D. C., Fiorino, M.,
1528 Gibson, J. K., Haseler, J., Hernandez, A., Kelly, G. A., Li, X., Onogi, K., Saarinen, S., Sokka,
1529 N., Allan, R. P., Andersson, E., Arpe, K., Balmaseda, M. A., Beljaars, A. C. M., Berg, L. V. D.,
1530 Bidlot, J., Bormann, N., Caires, S., Chevallier, F., Dethof, A., Dragosavac, M., Fisher, M.,
1531 Fuentes, M., Hagemann, S., Hólm, E., Hoskins, B. J., Isaksen, L., Janssen, P. A. E. M., Jenne, R.,
1532 McNally, A. P., Mahfouf, J. -F., Morcrette, J. -J., Rayner, N. A., Saunders, R. W., Simon, P.,
1533 Sterl, A., Trenberth, K. E., Untch, A., Vasiljevic, D., Viterbo, P., and Woollen, J.: The ERA-40
1534 re-analysis, Quarterly Journal of the Royal Meteorological Society, 131, 2961–3012,
1535 https://doi.org/10.1256/qj.04.176, 2005.

1536 Wahrhaftig, C., Stock, G. M., McCracken, R. G., Sasnett, P., and Cyr, A. J.: Extent of the Last
1537 Glacial Maximum (Tioga) glaciation in Yosemite National Park and vicinity, California, US
1538 Geological Survey Scientific Investigations Series Map, 3414, 2019.

1539 Wang, H., An, Z., Zhang, X., Shu, P., He, F., Liu, W., Lu, H., Ming, G., Liu, L., and Zhou, W.:
1540 Westerly and Laurentide Ice Sheet fluctuations during the Last Glacial Maximum, npj Climate
1541 and Atmospheric Science, 7, 2024.

1542 Waters, M. R.: Late Quaternary lacustrine history and paleoclimate significance of pluvial Lake
1543 Cochise, southeastern Arizona, Quaternary Research, 32, 1–11, 1989.

1544 Wong, C. I., Potter, G. L., Montañez, I. P., Otto-Bliesner, B. L., Behling, P., and Oster, J. L.:
1545 Evolution of moisture transport to the western U.S. during the last deglaciation, Geophysical
1546 Research Letters, 43, 3468–3477, https://doi.org/10.1002/2016GL068389, 2016.

1547 Ye, S., Cuzzone, J. K., Marcott, S. A., Licciardi, J. M., Ward, D. J., Heyman, J., and Quinn, D.
1548 P.: A quantitative assessment of snow shielding effects on surface exposure dating from a
1549 western North America ^{10}Be data compilation, Quaternary Geochronology, 76, 2023.

1550